ELSEVIER

Journal of Structural Geology 27 (2005) 1168–1189

JOURNAL OF STRUCTURAL GEOLOGY

www.elsevier.com/locate/jsg

Quantifying simultaneous discrete and distributed deformation

Eric Horsman*, Basil Tikoff

Department of Geology & Geophysics, University of Wisconsin—Madison, 1215 West Dayton Street, Madison, WI 53706, USA

Received 15 June 2003; received in revised form 5 January 2004
Available online 15 September 2004

Abstract

Most natural deformation involves simultaneous discrete deformation (e.g. faults) and distributed deformation (e.g. penetrative strain). In order to properly understand the bulk kinematics of a given deformation, the discrete and distributed components must be evaluated simultaneously. The displacement diagram method has previously been utilized to quantify strain accommodated by faults or other discrete surfaces. The same method is applicable to distributed deformation, such as ductilely deformed conglomerates, which are typically evaluated by finite strain analysis. By mathematically combining the gradients in the displacement fields of both the discrete and distributed components of deformation, the bulk deformation can be quantified. We apply this method to several examples that contain both distributed and discrete components, and characterize the bulk displacement field and finite strain for these deformed systems.

Keywords: Strain analysis; Deformation; Kinematics; Displacement

1. Introduction

An inconvenient characteristic of naturally deformed rocks is that they do not behave as idealized continua. Rather, earth materials develop discontinuities via slip or dissolution at the same time they experience bulk penetrative strain. S–C structures are just one example of this behavior (Fig. 1a). The shear surfaces (or C-bands) accommodate slip (discrete deformation). The S-domains, which lie between the shear surfaces, record penetrative strain (distributed deformation). Therefore, both discrete and distributed components must be evaluated to quantify the bulk deformation.

The characterization of discrete vs. distributed deformation depends on the scale of observation. The sign in Fig. 1b, viewed from 5 m (the approximate distance from which the photo was taken), is discretely deformed. Viewed from 50 m, the same deformation appears distributed. In the more complex S–C example, the shear surfaces appear as distributed deformation if viewed at higher magnification.

One approach to evaluate deformation is displacement field analysis, which has proved useful for many structural studies (e.g. Wojtal, 1989; Marrett and Allmendinger, 1990; Rouby et al., 1993; Little, 1996). This approach is typically used to calculate finite strain in brittle fault (discrete) systems (Wojtal, 1989). It is also possible to describe distributed deformation in terms of displacements (Ramsay and Huber, 1983, pp. 283–292). Consequently, the common 'language' of displacements can be used to analyze bulk deformation involving both discrete and distributed components. This approach works for deformation on all scales, as strain is scale independent.

In this study, we first show how distributed deformation is characterized using displacement diagrams. We then demonstrate how discrete and distributed components of deformation are combined to determine the bulk finite strain. The method is applied to several examples: (1) a two-dimensional example of a simple shear deformation, (2) a one-dimensional example of centimeter-scale deformation in carbonate, (3) a theoretical example of a bulk non-coaxial deformation, and (4) three-dimensional deformation within the San Andreas fault system.

* Corresponding author.
E-mail addresses: eric@geology.wisc.edu (E. Horsman), basil@geology.wisc.edu (B. Tikoff).

0191-8141/$ - see front matter © 2004 Elsevier Ltd. All rights reserved.
doi:10.1016/j.jsg.2004.08.001

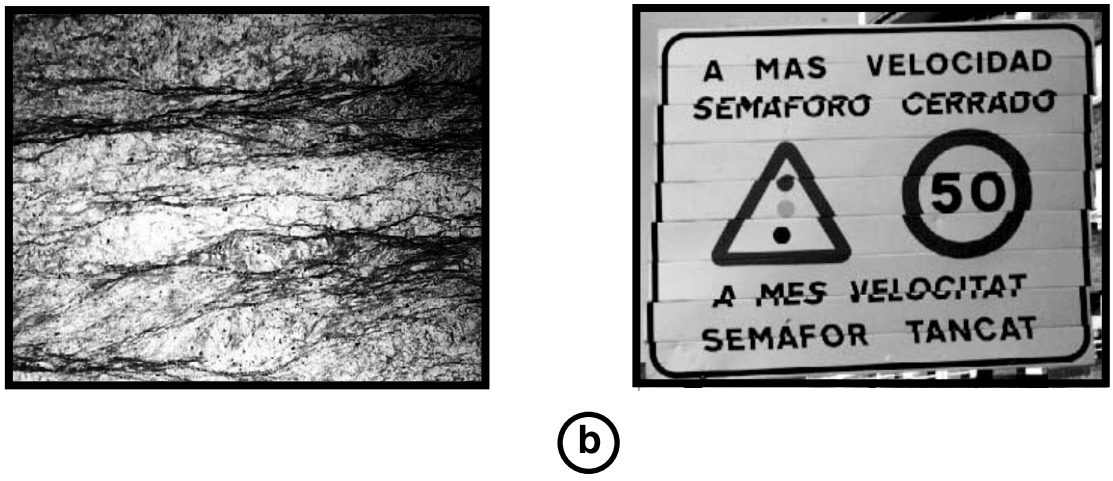

Fig. 1. Examples of deformed systems. The characterization of a deformation as discrete or distributed depends on the scale of observation. (a) Photomicrograph showing an S–C fabric in a sample from the Sandkraal sandstone formation, Kaaimaans inlier, near George, South Africa. Field of view ~4 mm. Elongate light-colored S domains, deforming in a distributed fashion are surrounded by dark C bands, which accommodate discrete slip. (b) Photograph of a deformed road sign in Tremp, Spain. Deformation appears discrete when viewed from 5 m, but distributed when viewed from 50 m.

2. Displacement diagrams

2.1. Displacement diagrams applied to discrete deformation

Within a deforming system, each material point moves from an initial position to a final position during deformation, defining a displacement vector. A displacement field is determined by calculating displacement vectors for a population of material points. Finite strain is caused by gradients of the displacement field. Several structural geology studies have utilized displacement field analysis (e.g. Cobbold, 1977; Wojtal, 1989; Marrett and Allmendinger, 1990; Rouby et al., 1993).

Displacement diagrams are one method of displacement field analysis and have been utilized to analyze bulk deformation accommodated by discrete structures (Wojtal, 1989; Little, 1996). A displacement diagram is a plot of cumulative displacement against spatial position, measured in an arbitrary coordinate system. Fig. 2a and b illustrates an example of discrete deformation, similar to the deformation in Fig. 1b. Fig. 2a shows the deformation of a box (dashed lines) to a series of fault blocks (solid lines). A displacement diagram for this deformation is given in Fig. 2b, in which displacement (U) is plotted against spatial position (y). The displacement in the x direction (U_x) of three material points (labeled 1–3) plot as individual points on this graph. The slope of the line through these points is the displacement gradient. The deformation matrix **D**, which describes the movement of material particles from the undeformed to the deformed state (Fig. 2c), is directly calculated from the displacement gradients. A general method for calculation of finite strain from displacement diagrams is given in Appendix A (for a more mathematically thorough discussion, see Wojtal (1989)). Means (1976) provides an excellent discussion of displacements, displacement gradients and matrices composed of these quantities. Mathematical symbols used throughout the paper are defined in Table 1.

Fig. 2d shows a deformation that is the exact reciprocal of the deformation in Fig. 2a. In Fig. 2d, the fault blocks define the initial state (dashed lines) and reciprocal deformation restores the system to its undeformed geometry (solid line). A displacement diagram describing this deformation is shown in Fig. 2e, in which reciprocal displacement (U') is plotted against spatial position (y'). The primes denote that the deformed state is the reference configuration (i.e. we follow a reciprocal or Eulerian approach—see Appendix B). Notice that, for this reciprocal deformation, displacement is in the negative x' direction, opposite that in Fig. 2b. The reciprocal displacement gradient is one component of the reciprocal deformation matrix **E** and, in this example, is responsible for the finite strain of the system. As the displacement gradients are of the same magnitude for both the forward and reciprocal deformations, the finite strain magnitude is the same for both deformations (Fig. 2a and d).

2.2. Displacement diagrams applied to distributed deformation

Although displacement diagrams have previously been used to analyze discrete deformation they can describe distributed deformation equally well. The deformation shown in Fig. 2f is the *distributed* equivalent of the reciprocal *discrete* deformation shown in Fig. 2d. As in Fig. 2d, reciprocal displacement is plotted against spatial position. However, rather than plotting as a series of material points that correspond to different fault blocks, the reciprocal displacement gradient plots as a continuous line of displaced material points. The reciprocal displacement gradients are the same for both the discrete and distributed deformation (cf. Fig. 2e and g). Consequently, these two deformations (Fig. 2d and f) have equivalent finite strains.

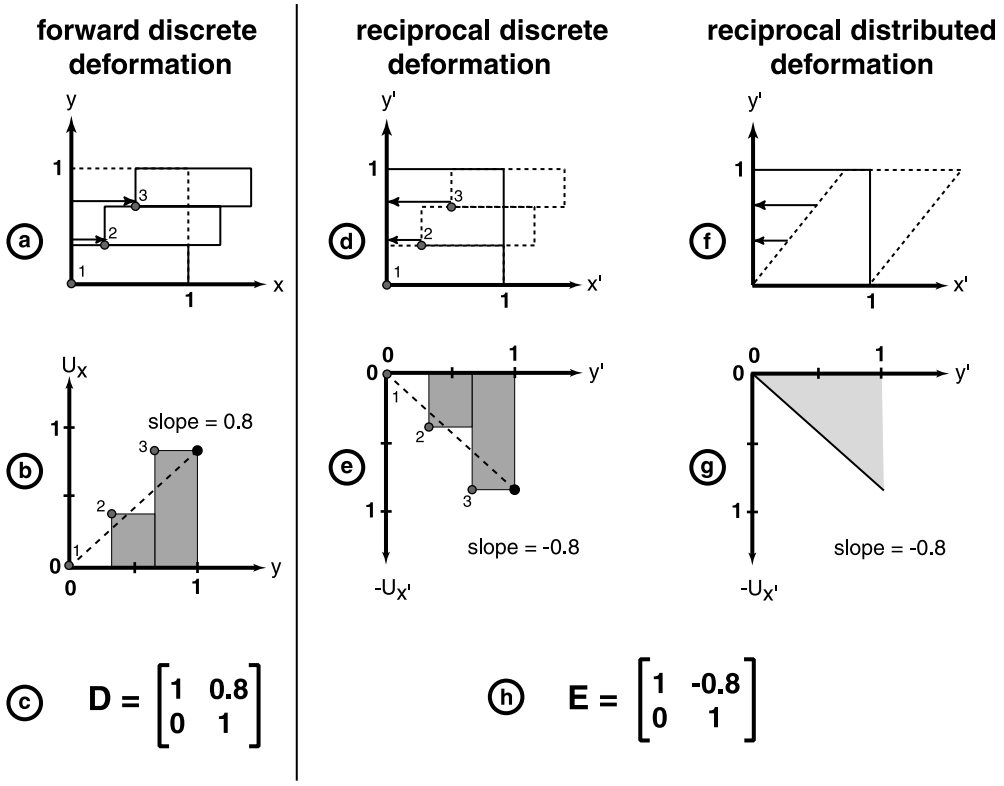

Fig. 2. Deformations and the corresponding displacement diagrams and deformation matrices. For the illustrations of the deformations ((a), (d) and (f)), the dashed lines refer to the initial geometry and the solid lines to the final geometry. (a) Forward discrete deformation, and (b) the corresponding displacement diagram that describes the deformation. In this case, cumulative displacement in the x direction is plotted against the y position. Points 1–3 (gray circles) correspond to points in (a). The gray boxes describe cumulative displacement. The displacement gradient (dashed line) is calculated by considering cumulative displacement over the entire length of the transect (black circle). (c) The deformation matrix **D** that mathematically describes (a). See Appendix A. (d) Reciprocal discrete deformation, and (e) the corresponding reciprocal displacement diagram. In this case, cumulative displacement in the x' direction is plotted against the y' position. Circles and displacement gradient are as in (b). (f) Reciprocal distributed deformation, and (g) the corresponding reciprocal displacement diagram. Again, cumulative displacement in the x' direction is plotted against the y' position. The shaded region describes cumulative reciprocal displacement. The displacement gradient is calculated by considering reciprocal cumulative displacement over the entire length of the transect. (h) The reciprocal deformation matrix **E** that mathematically describes either (d) or (f). See Appendix A.

2.3. Displacement diagrams and combined discrete and distributed deformation

The displacement diagram method considers *gradients* in displacement fields, rather than the fields themselves. Consequently, complex displacement fields composed of multiple component fields can be analyzed by summing displacement gradients from the component fields. Note that this simple summing is not possible for displacement fields themselves, as the resultant displacement field depends on the order in which the components occurred (e.g. simple shear followed by pure shear vs. pure shear followed by simple shear). Because it is possible to describe both the discrete and distributed components of any deformation

Table 1
Definitions of terminology

Mathematical notation	
U_i	Displacement in the i direction (undeformed system as reference)
j	Spatial position on the j transect (undeformed system as reference)
$U_{i'}$	Reciprocal displacement in the i' direction (deformed system as reference)
j'	Spatial position on the j' transect (deformed system as reference)
$\partial U_{i'}/\partial j'$	Reciprocal displacement gradient in the i' direction with respect to j' position
D	Deformation matrix
E	Reciprocal deformation matrix
G	Displacement gradient matrix
H	Reciprocal displacement gradient matrix
k_i	Stretch in the i direction
W_k	Kinematic vorticity number

with displacement fields, the displacement gradients of these component fields can be summed to yield a cumulative displacement gradient (Fig. 3). On a displacement diagram, the component displacement gradients (i.e. the slopes of lines) are added to yield the cumulative displacement gradient.

Although the deformations in Fig. 3 are shown for both a forward (Fig. 3a–e) and reciprocal (Fig. 3f–i) approach, we will utilize the reciprocal approach for the remainder of the manuscript. In general, the reciprocal approach is useful because it allows kinematic information to be extracted directly from naturally deformed rocks (Appendix B).

3. Two-dimensional example

We introduce the displacement diagram method using the well-known example of simple shear in a stack of computer cards (Fig. 4), which is kinematically identical to the example given in Fig. 3. This simple example is worked through in detail to demonstrate the method. For clarity, we consider the discrete and distributed components separately and combine them at the end of the analysis.

3.1. Analysis of two-dimensional systems

Displacement diagram analysis of a two-dimensional system requires two orthogonal transects (x' and y') across the deformed system. Generally, one of these transects is inscribed parallel to the bulk shear plane of the system. A displacement diagram must be created for cumulative displacement in the x' direction as measured along the x' transect ($U_{x'}$ vs. x'). Another displacement diagram is required for cumulative displacement in the y' direction as measured along the y' transect ($U_{y'}$ vs. y'). Both of these displacement diagrams record only shortening or elongation along the measured transect and, therefore, reflect the coaxial component of the deformation.

It is also possible to have displacement perpendicular to

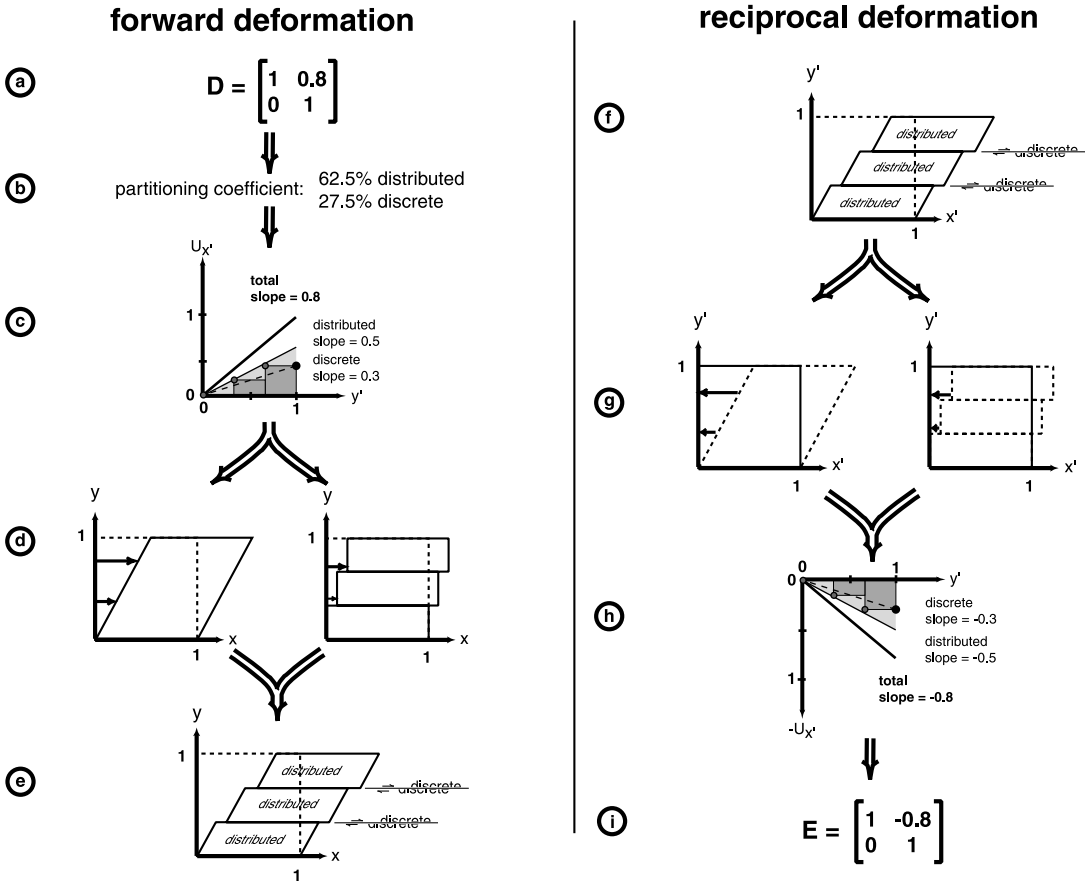

Fig. 3. Flow charts illustrating the difference between the forward and reciprocal approaches to the consideration of a deformation. From a forward modeling (Lagrangian) perspective, we (a) start with a deformation matrix, and (b) partition deformation into discrete and distributed components. These components are, (c) plotted on a displacement diagram as displacement gradients (see Fig. 2 for symbols). (d) The components of forward deformation are (e) graphically combined to yield a forward deformation whose bulk kinematics are described by the deformation matrix **D**. In contrast, analysis from a reciprocal (Eulerian) perspective starts with (f), the observed deformation. (g) This bulk deformation can be considered as a combination of both distributed and discrete components. (h) These components can be quantified and plotted (component slopes) and combined (total slope) on a displacement diagram. (i) The sum of the component displacement gradients relates directly to the reciprocal deformation matrix **E** that describes the reciprocal deformation necessary to transform the system back to its undeformed state.

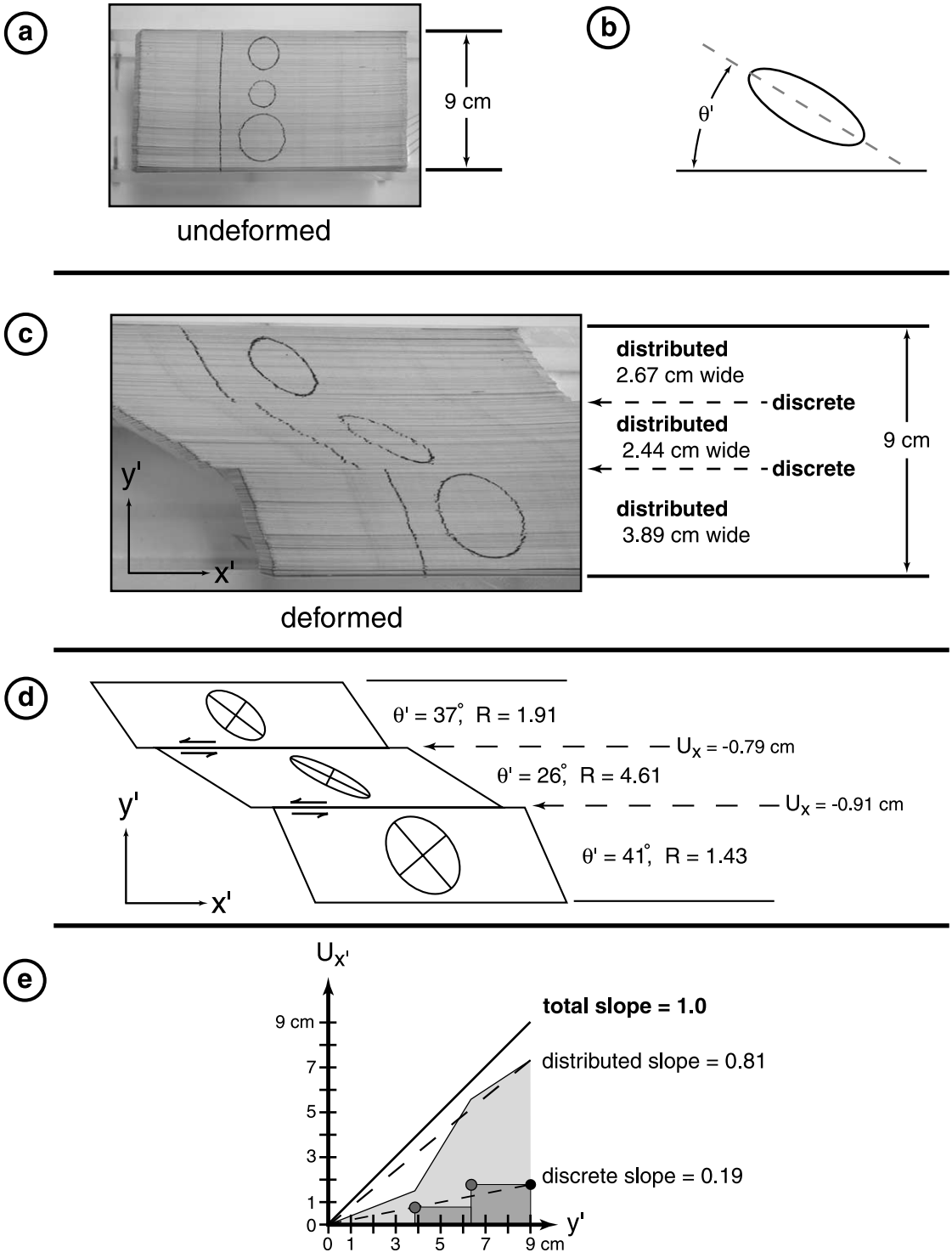

Fig. 4. A two-dimensional example of simple shear deformation involving both discrete and distributed components. (a) Photograph of an undeformed stack of computer cards, 9 cm thick. Three circles are drawn on the cards and a line is initially perpendicular to what will be the shear plane. (b) The angle θ' describes the orientation of the long axis of the finite strain ellipse with respect to the shear plane. (c) An annotated photograph of the computer cards after deformation. Three zones of distributed deformation are separated by two discrete faults. (d) A schematic line drawing of the deformation shown in (c). Values of R and θ' are shown for each zone of distributed deformation. Values of forward discrete displacement along each fault are also indicated. (e) The reciprocal displacement diagram that describes the retrodeformation. Dashed lines indicate component displacement gradients. Displacement gradient values are discussed in the main text.

the measured transect. This type of displacement reflects the non-coaxial component of deformation. Consequently, displacement diagrams must be created for cumulative displacement in the x' direction as measured along the y' transect ($U_{x'}$ vs. y') and for cumulative displacement in the y' direction as measured along the x' transect ($U_{y'}$ vs. x').

3.2. A simple shear example in detail

The system shown in Fig. 4 has three regions of distributed deformation separated by two faults. To begin, we inscribe orthogonal transects (x' and y'), with one transect (x' in this case) parallel to the bulk shear plane. Analysis of this system is simplified by the fact that we know the deformation was simple shear. Consequently, the deformation can be described with a single displacement diagram. The only displacement in the simple shear example is in the x' direction as measured along the y' transect ($U_{x'}$ vs. y'). There is no cumulative displacement in the x' direction as measured along the x' transect ($U_{x'}$ vs. x'), in the y' direction as measured along the y' transect ($U_{y'}$ vs. y'), or in the y' direction as measured along the x' transect ($U_{y'}$ vs. x'). Therefore, we can quantify deformation in the system by measuring displacement in the x' direction along the y' transect.

3.2.1. Distributed displacement

Each of the three zones of distributed deformation has a finite strain ellipse that we know accumulated in simple shear. For each zone, the observed aspect ratio (R) and the orientation of the strain ellipse's long axis (θ'; see Fig. 4b) can be used to calculate the forward deformation matrix that produced these values.

The bottom zone has a strain ellipse with an aspect ratio of $R=1.43$ and an orientation of $\theta'=41°$. Comparing these parameters with results from forward deformation models for simple shear, we find that the following forward distributed deformation matrix ($\mathbf{D}_{\text{distributed}}$) best matches our observations:

$$\mathbf{D}_{\text{distributed}} = \begin{bmatrix} 1 & -0.36 \\ 0 & 1 \end{bmatrix} \tag{1}$$

Once the forward distributed deformation matrix is known, we calculate the reciprocal distributed deformation matrix ($\mathbf{E}_{\text{distributed}}$) by finding the matrix inverse of $\mathbf{D}_{\text{distributed}}$:

$$\mathbf{E}_{\text{distributed}} = \mathbf{D}^{-1}_{\text{distributed}} = \begin{bmatrix} 1 & -0.36 \\ 0 & 1 \end{bmatrix}^{-1} = \begin{bmatrix} 1 & 0.36 \\ 0 & 1 \end{bmatrix}. \tag{2}$$

Applying $\mathbf{E}_{\text{distributed}}$ to the bottom zone would undeform the distributed deformation in that zone. This matrix is composed of two component matrices, the identity matrix ($\mathbf{I}$) and the reciprocal distributed displacement gradient matrix $\mathbf{H}_{\text{distributed}}$:

$$\mathbf{E}_{\text{distributed}} = \mathbf{I} + \mathbf{H}_{\text{distributed}}. \tag{3}$$

Rearranging and solving for $\mathbf{H}_{\text{distributed}}$ in this specific case:

$$\mathbf{H}_{\text{distributed}} = \mathbf{E}_{\text{distributed}} - \mathbf{I} = \begin{bmatrix} 1 & 0.36 \\ 0 & 1 \end{bmatrix} - \begin{bmatrix} 1 & 0 \\ 0 & 1 \end{bmatrix} = \begin{bmatrix} 0 & 0.36 \\ 0 & 0 \end{bmatrix}. \tag{4}$$

$\mathbf{H}_{\text{distributed}}$ describes the reciprocal displacement gradients for the bottommost zone of distributed deformation. Because of the simple shear nature of deformation, only one of these gradients is non-zero. This displacement gradient is plotted on the reciprocal displacement diagram in Fig. 4e. This diagram shows that, over the 3.89 cm thickness of the zone, this displacement gradient produces 1.40 cm ($=0.36\times3.89$ cm) of distributed displacement.

Analysis of the middle and top zones of distributed deformation follows these same procedures. For the middle zone, we find a reciprocal distributed displacement gradient of $\partial U_{x'}/\partial y' = 1.68$, which produces 4.10 cm of distributed displacement over the 2.33 cm thickness of the zone. For the top zone, we find a reciprocal distributed displacement gradient of $\partial U_{x'}/\partial y' = 0.66$, which produces 1.76 cm of distributed displacement over the 2.67 cm thickness of the zone. Both of these displacement gradients are plotted on the displacement diagram on Fig. 4e.

To calculate the bulk reciprocal distributed displacement gradient, we sum the reciprocal displacements from each zone and divide by the total thickness of the system.

$$\partial U_{x'}/\partial y' = (1.40 + 4.10 + 1.76)/9.0 = 0.81 \tag{5}$$

This displacement gradient is plotted as a dashed line on Fig. 4e. Because this is a simple shear deformation, we know that only one reciprocal distributed displacement gradient has a non-zero value. These quantities are:

$$\partial U_{x'}/\partial x' = 0, \tag{6a}$$

$$\partial U_{x'}/\partial y' = 0.81, \tag{6b}$$

$$\partial U_{y'}/\partial x' = 0, \tag{6c}$$

$$\partial U_{y'}/\partial y' = 0. \tag{6d}$$

Consequently, we know the cumulative reciprocal distributed displacement gradient matrix is:

$$\mathbf{H}_{\text{distributed}} = \begin{bmatrix} \partial U_{x'}/\partial x' & \partial U_{x'}/\partial y' \\ \partial U_{y'}/\partial x' & \partial U_{y'}/\partial y' \end{bmatrix} = \begin{bmatrix} 0 & 0.81 \\ 0 & 0 \end{bmatrix}. \tag{7}$$

3.2.2. Discrete displacements

Discrete displacement occurred along the two faults. The reciprocal displacement gradient for the discrete component is calculated by measuring the cumulative offset across these faults and dividing by the total thickness of the deformed system. The distance along the y' transect from the bottom edge of the system to the first fault is 3.89 cm. The measured discrete offset along this fault is 0.91 cm in the negative x' direction ($U_x = -0.91$ cm). However, we are interested in reciprocal displacement, which is identical in magnitude and opposite in sign (i.e. $U_{x'} = 0.91$ cm). The distance to the next fault is 2.44 cm; reciprocal displacement for that fault is $U_{x'} = 0.79$ cm. These reciprocal discrete displacements are plotted as gray circles on the reciprocal displacement diagram in Fig. 4e. The cumulative discrete displacement is plotted as gray boxes. To calculate the reciprocal discrete displacement gradient ($\partial U_{x'}/\partial y'$) we sum the displacements and divide by the thickness (9.0 cm) of the deformed zone:

$$\partial U_{x'}/\partial y' = (0.91 + 0.79)/9.0 = 0.19 \tag{8}$$

This reciprocal displacement gradient is plotted as a dashed line on Fig. 4e.

We can now calculate the reciprocal discrete displacement gradient matrix $\mathbf{H}_{\text{discrete}}$. Because this is a simple shear deformation, only one reciprocal discrete displacement gradient has a non-zero value. These quantities are:

$$\partial U_{x'}/\partial x' = 0, \tag{9a}$$

$$\partial U_{x'}/\partial y' = 0.19, \tag{9b}$$

$$\partial U_{y'}/\partial x' = 0, \tag{9c}$$

$$\partial U_{y'}/\partial y' = 0. \tag{9d}$$

Therefore the reciprocal discrete displacement gradient matrix is:

$$\mathbf{H}_{\text{discrete}} = \begin{bmatrix} \partial U_{x'}/\partial x' & \partial U_{x'}/\partial y' \\ \partial U_{y'}/\partial x' & \partial U_{y'}/\partial y' \end{bmatrix} = \begin{bmatrix} 0 & 0.19 \\ 0 & 0 \end{bmatrix}. \tag{10}$$

3.2.3. Quantifying combined distributed and discrete deformation

Summing the displacement gradient matrices from the discrete and distributed components yields the reciprocal displacement gradient matrix **H**. In general:

$$\mathbf{H} = \mathbf{H}_{\text{distributed}} + \mathbf{H}_{\text{discrete}}. \tag{11a}$$

For this specific case:

$$\mathbf{H} = \mathbf{H}_{\text{distributed}} + \mathbf{H}_{\text{discrete}} = \begin{bmatrix} 0 & 0.81 \\ 0 & 0 \end{bmatrix} + \begin{bmatrix} 0 & 0.19 \\ 0 & 0 \end{bmatrix} = \begin{bmatrix} 0 & 1 \\ 0 & 0 \end{bmatrix}. \tag{11b}$$

On the displacement diagram in Fig. 4e, this cumulative reciprocal displacement gradient ($\partial U_{x'}/\partial y' = 1$) is plotted as a solid line and is the sum of the two component displacement gradients that are plotted as dashed lines. The reciprocal deformation matrix is therefore:

$$\mathbf{E} = \mathbf{I} + \mathbf{H} = \begin{bmatrix} 1 & 0 \\ 0 & 1 \end{bmatrix} + \begin{bmatrix} 0 & 1 \\ 0 & 0 \end{bmatrix} = \begin{bmatrix} 1 & 1 \\ 0 & 1 \end{bmatrix}. \tag{12}$$

E describes the bulk reciprocal deformation of the entire system. The matrix inverse of **E** is the deformation matrix **D**:

$$\mathbf{D} = \mathbf{E}^{-1} = \begin{bmatrix} 1 & 1 \\ 0 & 1 \end{bmatrix}^{-1} = \begin{bmatrix} 1 & -1 \\ 0 & 1 \end{bmatrix}. \tag{13}$$

D describes the bulk forward deformation of the system, which resulted in the discrete and distributed components of the observed deformation. **D** allows us to characterize the deformation of the entire system with a single strain ellipse (in this case, $R = 2.6$ and $\theta' = 32°$) or with a bulk displacement field.

4. One-dimensional example

The simple shear example presented above is a good introductory example because (1) it contains only one non-zero displacement gradient term, and (2) the thickness of the deforming zone does not change during deformation. Quantification of shortening along a coordinate axis introduces complexity to the mathematical approach. To illustrate this, we next apply the method to a one-dimensional example of deformed carbonates (Fig. 5).

4.1. Analysis of one-dimensional systems

A one-dimensional system requires a single transect (x') inscribed parallel to the shortening or extension direction. Quantifying the deformation requires construction of a displacement diagram for cumulative reciprocal displacement in the x' direction ($U_{x'}$) as measured along the x' transect ($U_{x'}$ vs. x').

Deformed carbonates often contain regions characterized by discrete deformation features (e.g. stylolites) and regions of distributed deformation features (e.g. deformed fossils). At a magnified field of view the deformed fossils may undergo pressure solution and anisotropic volume loss (e.g. see fig. 7.12 in Ramsay and Huber, 1983). Consequently, we will make the assumption that the deformed shape of the finite strain markers results primarily from one-dimensional anisotropic solution transfer manifested by shortening in the x' direction (parallel to stylolite peaks) without a compensating perpendicular extension. This simplifying assumption allows us to consider the deformation of these markers as one-dimensional.

A slab of Indiana limestone is located in Room 178 in

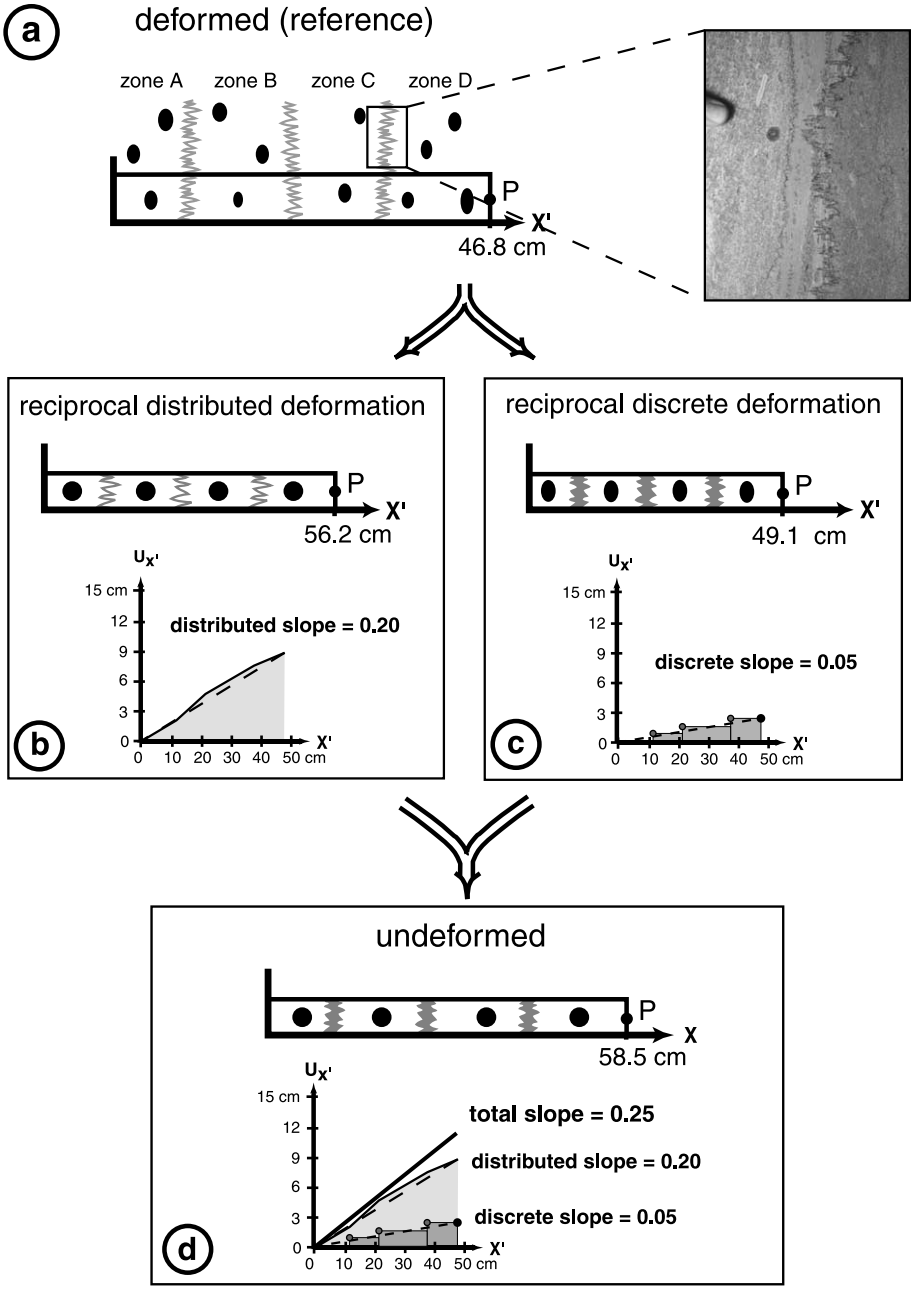

Fig. 5. Flow chart describing the construction of a reciprocal displacement diagram, using a one-dimensional system as an example. (a) Schematic diagram and inset photograph of the deformed carbonate in Room 178, Weeks Hall, University of Wisconsin. Fingertip for scale in the photograph. This is the deformed, or reference, state of the system showing both the strained markers (distributed deformation) and the stylolites (discrete deformation). (b) Schematic diagram of the system following reciprocal distributed deformation and the corresponding reciprocal displacement diagram. The shaded region describes cumulative displacement and the dashed line indicates the displacement gradient. (c) Schematic diagram of the system following reciprocal discrete deformation and the corresponding reciprocal displacement diagram. The shaded boxes describe cumulative displacement and the dashed line indicates the displacement gradient. (d) Schematic diagram of the system following both reciprocal distributed and reciprocal discrete deformation (i.e. this is the undeformed state) and the corresponding cumulative reciprocal displacement diagram. The total reciprocal displacement gradient is the sum of the two component gradients.

Weeks Hall at the University of Wisconsin. This slabbed sample (Fig. 5a) contains both stylolites (discrete deformation) and strained markers (distributed deformation). The deformation is assumed to result exclusively from burial compaction. A 46.8-cm-long section of this deformed carbonate was analyzed. All measurements used in our analysis are presented in Table 2.

4.2. Distributed displacement

To simplify the measurements and calculations, a transect line, x', is oriented parallel to the shortening direction recorded by the stylolite peaks (Fig. 5b). A transect line oblique to the shortening direction would require an additional transect perpendicular to the first.

Table 2
Measurements of discrete displacement and calculations of distributed displacement from deformed carbonate in Room 178, Weeks Hall, University of Wisconsin. These values are used to create the displacement diagrams in Fig. 5

Reciprocal distributed displacement						Reciprocal discrete displacement			
Interstylolite zone	Finite strain	x' stretch	Thickness (cm)	Reciprocal distributed displacement (cm)	Cumulative reciprocal distributed displacement (cm)	Stylolite	Position (cm)	Reciprocal discrete displacement (cm)	Cumulative reciprocal discrete displacement (cm)
A	1.20	0.83	10.35	2.07	2.07	1	10.35	0.78	0.78
B	1.25	0.8	10.58	2.65	4.72	2	20.95	0.67	1.45
C	1.17	0.85	16.61	2.82	7.54	3	37.55	0.85	2.30
D	1.2	0.83	9.22	1.84	9.38				

The three stylolite seams divide the carbonate into four regions of distributed deformation (labeled zones A–D on Fig. 5a). Within each zone the distributed deformation is recorded by strained markers (micritic blobs, crinoid stems, etc.; see inset on Fig. 5a). The finite strain in each of the zones was calculated using the center-to-center technique and the Fry method (our calculations are summarized in Table 2; for methodology see Ramsay and Huber (1983, pp. 107–113)).

The measured finite strain is not identical in each zone of distributed deformation. The initial length of each zone was calculated using the deformed length and the finite strain of the zone. By undeforming the observed finite strain ellipse, the initial length of the zone can be calculated. The difference between the final and initial lengths of each zone is the reciprocal distributed displacement for that zone. The displacements from all the zones were summed on a displacement diagram to yield a bulk reciprocal distributed displacement for the entire area.

For example, zone A is 10.35 cm across and records a stretch of 0.83 parallel to the transect. Therefore, zone A was originally 12.4 cm ($=10.35\text{ cm}\times(1/0.83)$) across and the endpoints of the zone extend 2.1 cm during reciprocal deformation. We sum the reciprocal distributed displacements for all four zones and consider the resulting movement of the point P. This point is displaced 9.4 cm in the x' direction ($U_{x'}=9.4$) due to the cumulative reciprocal distributed displacement for all four zones. We are calculating the reciprocal displacement (i.e. undeforming the rock) and therefore reciprocal displacement is in the positive x' direction.

4.3. Distributed displacement gradient

The reciprocal displacement gradient (i.e. slope of the line on the reciprocal displacement diagram) is the cumulative reciprocal distributed displacement ($U_{x'}$) divided by the deformed length (x') of the carbonate: $U_{x'}/x'=9.4/46.8=0.20$. This reciprocal displacement gradient is plotted on a reciprocal displacement diagram on Fig. 5b.

The finite strain corresponding to the distributed displacement gradient can be quantified using linear algebra (see Appendix A for a more detailed treatment). The reciprocal distributed displacement gradient matrix in one dimension is simply the calculated displacement gradient ($\mathbf{H}_{\text{distributed}}=[0.20]$).

4.4. Discrete displacement

For each stylolite seam, the distance between stylolite peaks yields a minimum estimate of the discrete displacement. The same transect utilized for the distributed deformation is used for analysis of the discrete deformation. Starting at the left end of the x' transect (Fig. 5c), we measure the distance to the first stylolite seam (10.35 cm; stylolite 1) and the amount of shortening (0.78 cm). The process is repeated for all stylolite seams. Summing the displacement on all stylolite seams (Table 2), we calculate 2.3 cm of cumulative displacement due to pressure solution. We again consider the displacement of point P to determine reciprocal displacement. P moves 2.3 cm in the positive x' direction due to the reciprocal discrete displacement and therefore $U_{x'}=2.3$.

4.5. Discrete displacement gradient

To quantify the deformation of the system due to discrete deformation we can calculate a reciprocal displacement gradient by considering the movement of point P (Fig. 5c) during the reciprocal deformation of the stylolite seams. This point is displaced 2.3 cm in the positive x' direction ($U_{x'}=2.3$) over the transect distance of 46.8 cm ($x'=46.8$). Consequently, the reciprocal discrete displacement gradient is the cumulative reciprocal displacement across the stylolites divided by the initial transect length: $U_{x'}/x'=2.3/46.8=0.05$. This reciprocal displacement gradient is plotted on a reciprocal displacement diagram in Fig. 5c.

This displacement gradient produced the strain that accumulated through discrete displacement. The reciprocal discrete displacement gradient matrix $\mathbf{H}_{\text{discrete}}$ in one dimension is the calculated displacement gradient ($\mathbf{H}_{\text{discrete}}=[0.05]$).

4.6. Quantifying combined distributed and discrete deformation

We can now calculate the initial length of the system. Combining the discrete and distributed components of the total deformation is straightforward with the reciprocal displacement diagram. In this specific example:

$$\mathbf{H} = \mathbf{H}_{\text{distributed}} + \mathbf{H}_{\text{discrete}} = [0.20] + [0.05] = [0.25]. \quad (14)$$

This bulk reciprocal displacement gradient matrix is the sum of the component displacement gradient matrices (Fig. 5d). The reciprocal deformation matrix **E** is the sum of the identity matrix and **H**:

$$\mathbf{E} = \mathbf{I} + \mathbf{H} = [1] + [0.25] = [1.25]. \quad (15)$$

Multiplying **E** by the deformed transect length (46.8 cm), we calculate the undeformed transect length of 58.5 cm (= [1.25]×46.8 cm). Thus, we have accounted simultaneously for both the discrete and distributed components of the deformation. We can quantify the bulk length change of the carbonate during forward deformation by calculating the determinant of **D**, where **D** is the matrix inverse of **E**:

$$\mathbf{D} = \mathbf{E}^{-1} = [1.25]^{-1} = [0.8]. \quad (16)$$

As det(**D**)=0.8 this one-dimensional system lost 20% of its length as a result of the combined discrete and distributed components of the bulk deformation.

5. A two-dimensional general shear example

5.1. Two difficulties for two-dimensional analysis

The two previous examples are relatively straightforward, containing only simple shear or uniaxial shortening. When pure shear and simple shear components are combined during a single deformation, mathematical complexities arise. To use the displacement diagram method in such a case, we need to address (1) rotation, particularly for the distributed component of deformation; and (2) the effect of the pure shear component on the calculation of discrete deformation. We address these in order below.

5.1.1. The effect of rotation on discrete deformation

To evaluate the discrete component of a given deformation in two or three dimensions, it is necessary to address the rotation of faults. Rotation of faults is observed in experimental models (e.g. Cobbold, 1977) and is required for realistic tectonic models (e.g. Luyendyk, 1991). Geological markers (e.g. sedimentary bedding) and paleomagnetic analysis allow evaluation of finite rotation. If these rotations are determined, displacement fields can be constructed to accommodate these rotational displacements in addition to the strain-induced displacements. Gradients of these rotational displacement fields can be summed along with gradients of the strain-related fields to properly quantify the bulk deformation of the system. However, for the purposes of this example, we will assume that the faults do not rotate.

5.1.2. The effect of rotation on distributed deformation

For the distributed components of deformation in our previous examples (simple shear and uniaxial shortening), we assumed the amount of coaxiality vs. non-coaxiality (i.e. shear-induced vorticity; Lister and Williams, 1983) in the system. In general, however, one does not know the amount of coaxiality of a deformed region a priori because finite strain does not provide information about the deformation path. Consequently, the displacement diagram method can be difficult to implement accurately because the particular displacement gradient values are unknown.

This problem is resolved by evaluating the deformation path, which has long been a subject of interest in structural geology (e.g. Elliott, 1972; Means, 1976). In particular, we utilize vorticity analysis, which quantifies the degree of coaxiality within a deforming rock mass. The structural geology literature commonly uses the kinematic vorticity (W_k; Truesdell, 1953) to quantify coaxiality. For the case of two-dimensional deformation, one can distinguish a coaxial deformation with no rotation (pure shear: $W_k=0$), non-coaxial deformations with combinations of pure shear and simple shear ($1>W_k>0$), and simple shear ($W_k=1$). W_k is inherently an infinitesimal quantity, therefore geological analysis solves for a 'bulk' vorticity, or W_n (e.g. Passchier, 1988). In fact, W_n is the preferable quantity for our 'bulk displacement' approach, as it provides an integrated vorticity for the entire deformation.

Although there are limitations to vorticity analysis (e.g. Tikoff and Fossen, 1995), it has proved extremely useful in determining the deformation path from deformed rock. These approaches include interpretations of shear bands (Bobyarchick, 1986), deformed makers in shear zones (Srivastava et al., 1995), porphyroblast rotation (Ghosh, 1987; Vissers, 1989; Simpson and De Paor, 1993), porphyroclast interaction (Tikoff and Teyssier, 1994), deformed sets of veins and dikes (Passchier and Urai, 1988; Daczko et al., 2001), crystallographic fabrics (Law et al., 1984; Wallis, 1992; Erskine et al., 1993), tension gashes (Tikoff and Fossen, 1995), and orientation of finite strain with respect to shear zone boundaries (Fossen and Tikoff, 1993; Bailey and Eyster, 2003).

5.1.3. The effect of the pure shear component on the calculation of discrete deformation

In most deformed systems that contain a coaxial component of deformation, the distance between the faults changes during deformation as a result of the deformation of the blocks between the faults. This change in fault spacing is demonstrated in Fig. 6. The measured cumulative slip on the

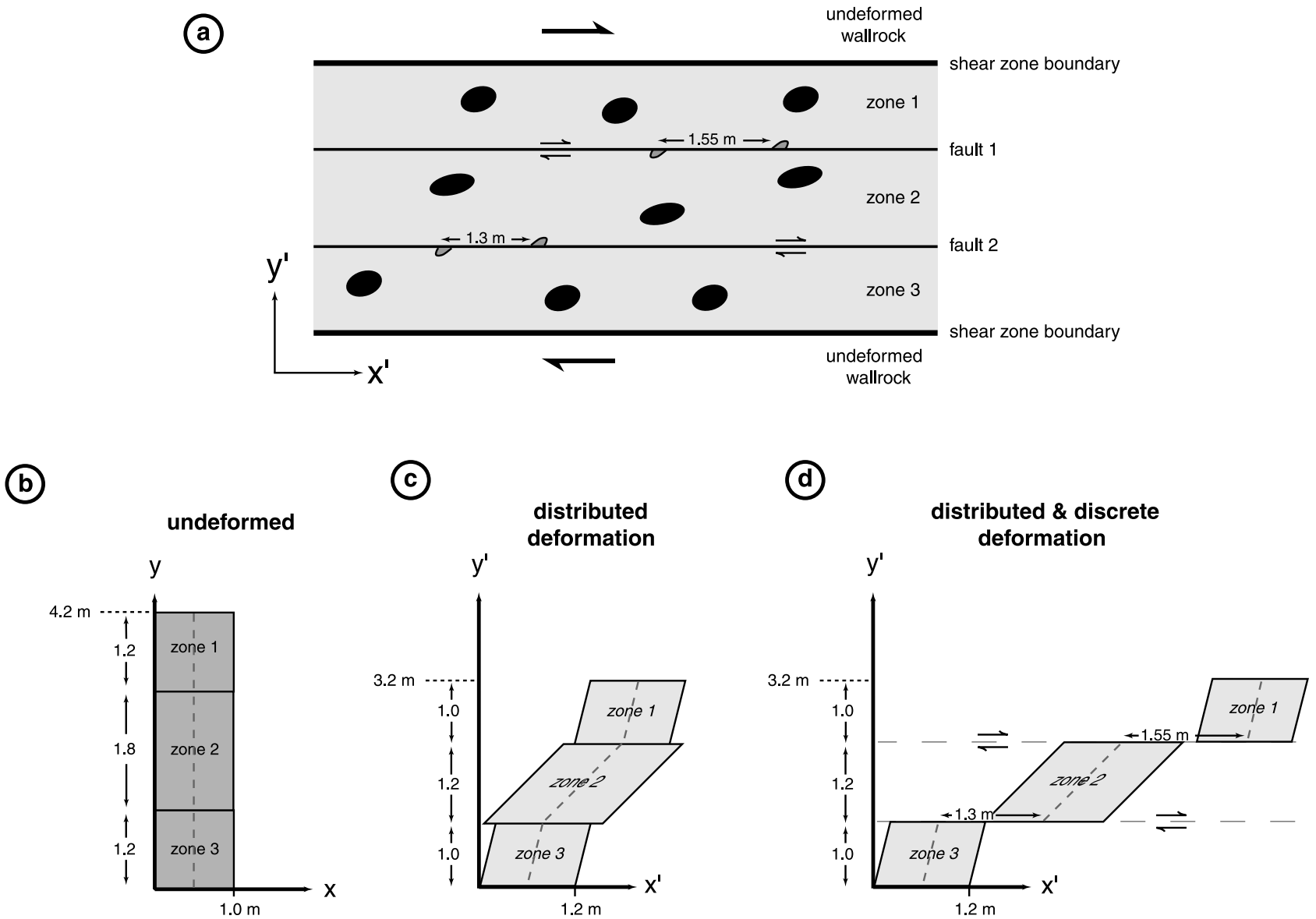

Fig. 6. A schematic example of a plane strain shear zone that includes both discrete and distributed components of deformation. (a) The shear zone is composed of three component zones of distributed deformation separated by two discrete faults. (b) An illustration of the thickness of each of the three component distributed zones prior to deformation. These thicknesses were calculated by undeforming the finite strain recorded in each zone (see text for calculations). (c) An illustration of the system following distributed deformation only. (d) An illustration of the system following both distributed and discrete deformation. Note that (1) these components were active simultaneously and we separate them only for clarity of discussion, and (2) the discrete offset is assumed to be due entirely to straightforward fault slip—slip on the surfaces due to differential finite strain in the adjacent blocks is ignored.

two faults is $U_{x'} = -2.85$ m. The faults start at a spatial position of $y' = 1.2$ and $y' = 3.0$ when the entire system is 4.2 m thick. The faults end at spatial positions of $y' = 1.0$ m and $y' = 2.2$ m when the system is 3.2 m thick. The calculated reciprocal displacement gradient depends on whether the post- or pre-deformational system thickness is used. If the observed post-deformational system thickness is used, then $\partial U_{x'}/\partial y' = -2.85/3.2 = -0.89$, whereas if the pre-deformational thickness is used, the $\partial U_{x'}/\partial y' = -2.85/4.2 = -0.68$. The pre-deformation system thickness leads to the correct reciprocal discrete displacement gradient. Using the post-deformation thickness results in a displacement gradient too large in proportion to the coaxial component of the deformation.

This problem arises in the application of the displacement diagram method to any system of combined discrete and distributed deformation whose kinematics includes both coaxial and non-coaxial components. Because our earlier examples were non-coaxial (simple shear in the card deck) or one-dimensional (deformed carbonates), this problem was not of concern. However, many examples of deformed systems include both coaxial and non-coaxial components. Consequently, it is necessary to first reconstruct the coaxial component of distributed component of deformation before calculating the displacement gradients associated with the discrete component of deformation. We apply this methodology in the analysis below.

5.1.4. Differential finite strain in adjacent fault-bounded blocks

An additional complication arises in systems involving zones of distributed deformation that record different finite strains and are separated by surfaces of discrete displacement. For example, in Fig. 6c, the middle block records a larger amount of finite strain than the outer blocks. The surfaces between the blocks necessarily have discrete offset due to this differential finite strain. Consequently, the discrete displacement measured from offset markers in Fig. 6a involves components from differential distributed finite strain between the blocks (Fig. 6c) *and* from straightforward slip along the faults. This complication is compounded by the fact that the offset due to differential finite strain will vary systematically along the surface, from zero at the center of the system to a maximum at the edges. Analysis of several offset markers along such a surface might provide sufficient information to estimate the importance of offset due to differential finite strain vs. straightforward fault slip. However, in general, this complication must be accepted as an inconvenience and displacement diagram results for these systems are imperfect at best. In the following analysis of the deformed system shown in Fig. 6, we lack sufficient information to analyze the relative importance of differential finite strain vs. fault slip. Consequently, we have ignored the offset due to differential distributed finite strain between the blocks.

5.2. Example of shear zone analysis

A schematic shear zone is presented in Fig. 6. The shear zone displays both a discrete component of deformation, denoted by the offset markers, and a distributed component, which causes deformation of the initially circular markers within the shear zone. Kinematically, the bulk deformation involved both coaxial and non-coaxial components, though we do not know in what proportion. We demonstrate below that vorticity analysis is one method of addressing the rotational component of the deformation. Correct retro-deformation of this shear zone also requires consideration of the changing thickness of the system due to the coaxial component of the deformation. We assume the shear zone neither gained nor lost volume during deformation, and that the deformation is plane strain.

5.2.1. Distributed displacement

Three zones of distributed deformation are separated by two faults. The inner zone of distributed deformation (zone 2) has a higher finite strain than is observed in the two identical outer zones of distributed deformation (zones 1 and 2).

5.2.1.1. Calculation for zone 2. We use the observed finite strain in each component shear zone to estimate vorticity, using the R_s vs. θ' method (e.g. Bailey and Eyster, 2003). On Fig. 6, zone 2 (the highest strain zone) has a finite strain ellipse with an aspect ratio of $R = 3.45$ at an orientation of $\theta' = 12.8°$ to the shear zone boundary. The R_s vs. θ' method provides a vorticity value of $W_k = 0.75$. In addition, one can uniquely determine the components of simultaneous pure shear ($k_x = 1.5$) and simple shear ($\gamma = 1.0$) that caused this deformation (e.g. fig. 3 of Tikoff and Fossen, 1995). The plane strain assumption requires that $k_y = 1/k_x = 0.67$. We emphasize that finite strain markers are not essential, as an estimate of principal finite strain orientations (e.g. foliation, lineation) and kinematic vorticity would provide sufficient information for the analysis.

With the strain values calculated above, we can characterize the shear strain caused by the distributed deformation. Tikoff and Fossen (1993) show that, in cases of simultaneous pure and simple shear, the shear strain term Γ is a function of the simple shear component (γ) and the pure shear components (k_x and k_y) of deformation:

$$\Gamma = \frac{\gamma(k_x - k_y)}{\ln(k_x/k_y)}. \tag{17}$$

For zone 2:

$$\Gamma = \frac{1(1.5 - 0.67)}{\ln(1.5/0.67)} = 1.03. \tag{18}$$

Using the relationships:

$$k_x = 1 + \partial U_x/\partial x, \tag{19a}$$

$$\Gamma = \partial U_x/\partial y, \tag{19b}$$

$$k_y = 1/k_x = 1 + \partial U_y/\partial y, \tag{19c}$$

we calculate the forward distributed displacement gradients, such that:

$$\partial U_x/\partial x = 0.5, \tag{20a}$$

$$\partial U_x/\partial y = 1.03, \tag{20b}$$

$$\partial U_y/\partial x = 0, \tag{20c}$$

$$\partial U_y/\partial y = -0.33. \tag{20d}$$

The corresponding distributed displacement gradient matrix is:

$$\mathbf{G}_{\text{distributed}} = \begin{bmatrix} 0.5 & 1.03 \\ 0 & -0.33 \end{bmatrix}. \tag{21}$$

The next step is to calculate the reciprocal distributed displacement gradient matrix $\mathbf{H}_{\text{distributed}}$. The most instructive way to accomplish this is to (1) calculate the forward distributed deformation matrix $\mathbf{D}_{\text{distributed}}$ by summing $\mathbf{G}_{\text{distributed}}$ and the identity matrix, (2) take the matrix inverse of $\mathbf{D}_{\text{distributed}}$, which yields the reciprocal distributed deformation matrix $\mathbf{E}_{\text{distributed}}$, and (3) subtract the identity matrix from this to yield $\mathbf{H}_{\text{distributed}}$, the reciprocal distributed displacement gradient matrix:

$$\begin{aligned}\mathbf{D}_{\text{distributed}} &= \mathbf{G}_{\text{distributed}} + \mathbf{I} \\ &= \begin{bmatrix} 0.5 & 1.03 \\ 0 & -0.33 \end{bmatrix} + \begin{bmatrix} 1 & 0 \\ 0 & 1 \end{bmatrix} \\ &= \begin{bmatrix} 1.5 & 1.03 \\ 0 & 0.67 \end{bmatrix},\end{aligned} \tag{22}$$

$$\begin{aligned}\mathbf{E}_{\text{distributed}} &= \mathbf{D}^{-1}_{\text{distributed}} = \begin{bmatrix} 1.5 & 1.03 \\ 0 & 0.67 \end{bmatrix}^{-1} \\ &= \begin{bmatrix} 0.67 & -1.03 \\ 0 & 1.5 \end{bmatrix},\end{aligned} \tag{23}$$

$$\begin{aligned}\mathbf{H}_{\text{distributed}} &= \mathbf{E}_{\text{distributed}} - \mathbf{I} \\ &= \begin{bmatrix} 0.67 & -1.03 \\ 0 & 1.5 \end{bmatrix} - \begin{bmatrix} 1 & 0 \\ 0 & 1 \end{bmatrix} \\ &= \begin{bmatrix} -0.33 & -1.03 \\ 0 & 0.5 \end{bmatrix}.\end{aligned} \tag{24}$$

Thus, the reciprocal distributed displacement gradients for zone 2 are:

$$\partial U_{x'}/\partial x' = -0.33, \tag{25a}$$

$$\partial U_{x'}/\partial y' = -1.03, \tag{25b}$$

$$\partial U_{y'}/\partial x' = 0, \tag{25c}$$

$$\partial U_{y'}/\partial y' = 0.5. \tag{25d}$$

5.2.1.2. Restoration of the original thickness. As discussed in Section 5.1.3, we must restore the deformed system to its initial thickness in order to calculate the correct reciprocal discrete displacement gradient. We can accomplish this task by restoring each of the three zones of distributed deformation to its initial thickness. The reciprocal distributed deformation matrix $\mathbf{E}_{\text{distributed}}$ for each zone can be used for this purpose.

The original thickness of zone 2 can be calculated by considering how this reciprocal distributed deformation matrix would affect the thickness of this 1.2-m-thick zone. Inspection of this matrix shows that only the $\partial U_{x'}/\partial y'$ component of $\mathbf{E}_{\text{distributed}}$ (Eq. (23)) will affect the thickness of the zone. We can therefore calculate that zone 2 was initially $1.2 \times 1.5 = 1.8$ m thick.

5.2.1.3. Calculation for zones 1 and 3. We can find reciprocal deformation matrices for zones 1 and 3 by following the same procedure as above. These zones exhibit identical finite strain and are characterized by an $R = 1.56$ and $\theta' = 14°$, which implies a $W_k = 0.30$. This vorticity corresponds to a pure shear component of $k_x = 1.2$ and a simple shear component of $\gamma = 0.25$. The plane strain assumption requires that $k_y = 0.83$ and Eq. (17) allows us to calculate $\Gamma = 0.25$. Using the relationships in Eq. (19a)–(19c), we calculate the forward distributed displacement gradients, such that:

$$\partial U_x/\partial x = 0.2, \tag{26a}$$

$$\partial U_x/\partial y = 0.25, \tag{26b}$$

$$\partial U_y/\partial x = 0, \tag{26c}$$

$$\partial U_y/\partial y = -0.17. \tag{26d}$$

The corresponding distributed displacement gradient matrix is:

$$\mathbf{G}_{\text{distributed}} = \begin{bmatrix} 0.2 & 0.25 \\ 0 & -0.17 \end{bmatrix}. \tag{27}$$

Again, we want to calculate reciprocal displacement gradients. Following the process shown in Eqs. (22)–(24), we find that the reciprocal distributed displacement gradient matrix for zones 1 and 3 is:

$$\mathbf{H}_{\text{distributed}} = \begin{bmatrix} -0.17 & -0.25 \\ 0 & .20 \end{bmatrix}. \tag{28}$$

Thus, the reciprocal distributed displacement gradients

for zones 1 and 3 are:

$$\partial U_{x'}/\partial x' = -0.17, \tag{29a}$$

$$\partial U_{x'}/\partial y' = -0.25, \tag{29b}$$

$$\partial U_{y'}/\partial x' = 0, \tag{29c}$$

$$\partial U_{y'}/\partial y' = 0.2. \tag{29d}$$

5.2.1.4. Restoration of the original thickness. The original thickness of zones 1 and 3 can be calculated by considering how the $\mathbf{E}_{\text{distributed}}$ corresponding to the reciprocal distributed displacement gradients in Eq. (29a)–(29d) would affect the thickness of these 1.0-m-thick zones. As we found for zone 2, inspection of this matrix shows that only the $\partial U_{x'}/\partial y'$ component of the matrix will affect the thickness of the zone. We can therefore calculate that each zone was initially $1.0 \times 1.2 = 1.2$ m thick. Having analyzed the distributed deformation throughout the entire system, we can calculate the initial thickness of the system. Summing the initial thicknesses of the zones, we find that the original system was $1.2 + 1.8 + 1.2 = 4.2$ m thick.

5.2.1.5. Bulk reciprocal distributed displacement. Finally, we must calculate the reciprocal distributed displacement gradient matrix $\mathbf{H}_{\text{distributed}}$ for the entire system. We now have sufficient information to calculate the forward distributed deformation matrix $\mathbf{D}_{\text{distributed}}$ for the entire system, from which we can calculate the system's $\mathbf{H}_{\text{distributed}}$, as shown for zone 2 in Eqs. (22)–(24). Beginning with the k_y term of $\mathbf{D}_{\text{distributed}}$, we know that the zone as a whole shortened from 4.2 to 3.2 m thick during deformation. The k_y term is therefore $3.2/4.2 = 0.76$. Because we assume this was a constant volume deformation, k_x is therefore constrained to be $1/k_y = 1.32$.

We can calculate the simple shear term of $\mathbf{D}_{\text{distributed}}$ by (1) summing the appropriate displacements produced by each zone's Γ term, and (2) dividing this net displacement by the thickness of the entire system. To calculate the displacements, we multiply each zone's Γ by the initial thickness of that zone. Consequently, the appropriate displacements for the three zones are:

$$\text{Zone 1}: \quad \Gamma \times y' = 0.25 \times 1.2 \text{ m} = 0.3 \text{ m}, \tag{30a}$$

$$\text{Zone 2}: \quad \Gamma \times y' = 1.03 \times 1.8 \text{ m} = 1.85 \text{ m}, \tag{30b}$$

$$\text{Zone 3}: \quad \Gamma \times y' = 0.25 \times 1.2 \text{ m} = 0.3 \text{ m}. \tag{30c}$$

Thus, the net distributed displacement $0.3 + 1.85 + 0.3 = 2.45$ m. Dividing this value by the thickness of the entire system we find that $\Gamma = 2.45/4.2 = 0.58$. We now have all of the terms of the forward distributed deformation matrix:

$$\mathbf{D}_{\text{distributed}} = \begin{bmatrix} 1.32 & 0.58 \\ 0 & 0.76 \end{bmatrix}. \tag{31}$$

This matrix describes the forward deformation of the distributed component of the entire system. From this matrix we can calculate the reciprocal distributed displacement gradient matrix $\mathbf{H}_{\text{distributed}}$ for the entire system by following the same procedure shown in Eqs. (23) and (24). Doing this, we find that:

$$\mathbf{H}_{\text{distributed}} = \begin{bmatrix} -0.24 & -0.58 \\ 0 & 0.32 \end{bmatrix}. \tag{32}$$

5.2.2. Discrete displacement

The discrete component of deformation is relatively easy to characterize, once the original thicknesses are known. Measuring along the y' transect, the cumulative reciprocal displacement on the discrete zones is -2.85 m ($U_{x'} = -1.55 + -1.3$). Consequently, $\partial U_{x'}/\partial y' = -2.85/4.2 = -0.68$. Notice that the reciprocal displacement gradient was calculated by dividing the cumulative reciprocal displacement by the *initial* thickness of the system for the reasons described in Section 5.1.3. The reciprocal discrete displacement gradient matrix is:

$$\mathbf{H}_{\text{discrete}} = \begin{bmatrix} 0 & -0.68 \\ 0 & 0 \end{bmatrix}. \tag{33}$$

5.2.3. Combined discrete and distributed displacement

We can now combine the reciprocal discrete and distributed displacement gradient matrices:

$$\begin{aligned} \mathbf{H} &= \mathbf{H}_{\text{distributed}} + \mathbf{H}_{\text{discrete}} \\ &= \begin{bmatrix} -0.24 & -0.58 \\ 0 & 0.32 \end{bmatrix} + \begin{bmatrix} 0 & -0.68 \\ 0 & 0 \end{bmatrix} \\ &= \begin{bmatrix} -0.24 & -1.26 \\ 0 & 0.32 \end{bmatrix}. \end{aligned} \tag{34}$$

The reciprocal deformation matrix is therefore:

$$\begin{aligned} \mathbf{E} = \mathbf{I} + \mathbf{H} &= \begin{bmatrix} 1 & 0 \\ 0 & 1 \end{bmatrix} + \begin{bmatrix} -0.24 & -1.26 \\ 0 & 0.32 \end{bmatrix} \\ &= \begin{bmatrix} 0.76 & -1.26 \\ 0 & 1.32 \end{bmatrix}. \end{aligned} \tag{35}$$

From $\mathbf{E}$ we calculate the deformation matrix:

$$\mathbf{D} = \mathbf{E}^{-1} = \begin{bmatrix} 0.76 & -1.26 \\ 0 & 1.32 \end{bmatrix}^{-1} = \begin{bmatrix} 1.32 & 1.26 \\ 0 & 0.76 \end{bmatrix}. \tag{36}$$

$\mathbf{D}$ describes the bulk forward deformation of the entire

system due to both the discrete and distributed components of the deformation.

6. Application to the San Andreas Fault system

6.1. Finite strain vs. neotectonic deformation

All of the above examples employ finite strain data for the displacement diagram method analysis. The same methodology can be applied to neotectonic settings with considerably less difficulty. There are two primary reasons for this relative simplicity: (1) the boundary conditions of deformation are well known, and (2) one can directly use displacements—both rates from geodesy and offset markers from geology—to calculate bulk deformation. Below, we apply the displacement diagram method to a portion of the creeping segment of the San Andreas Fault (SAF) system in central California.

One caveat to our analysis is that a geodetic signal may contain components of elastic strain accumulation that will be released during the earthquake cycle (e.g. Thatcher, 1995). The observations we use for this analysis are primarily from the region adjacent to the creeping segment of the SAF, in which the short-term offset is approximately the same as the long-term offset rates on 'locked' segments of the SAF. Consequently, relatively little elastic strain has the opportunity to accumulate and, to a first approximation, distributed deformation across this zone reflects permanent deformation of the crust adjacent to the fault. Further, the geodetic rates are compatible with estimates of distributed transpressional deformation throughout western California, determined from fold axis orientations adjacent to the SAF (e.g. Jamison, 1991; Tikoff and Peterson, 1998; Teyssier and Tikoff, 1998).

6.2. Analysis of three-dimensional systems

Analysis of a three-dimensional deformation requires three mutually orthogonal transects and nine displacement diagrams. Along each transect, three directions of displacement must be measured: displacement parallel to the transect (reflecting the pure shear component of deformation) and shear displacement parallel to each of the other two transects (reflecting the simple shear component of deformation).

Some three-dimensional deformations, however, can be analyzed more simply if constant volume is assumed (e.g. Little, 1996). A three-dimensional deformation can be characterized by (1) analyzing a plane within the system using four displacement diagrams, (2) calculating the two-dimensional deformation matrix for that plane, (3) using the determinant of the matrix to calculate area change within the plane, and (4) creating a three-dimensional matrix that satisfies the constant volume system assumption. This method is not applicable to systems that have a component of simple shear movement perpendicular to the analyzed plane (i.e. the plane in which the two-dimensional deformation matrix was calculated). Little (1996) used the constant volume assumption to conduct a three-dimensional displacement diagram analysis of a segment of the Marlborough fault system in South Island, New Zealand. We, too, will utilize this assumption for our analysis of the SAF.

6.3. Geological background

The well-documented geology in central California provides an opportunity to apply the displacement diagram method to a natural geological example (Fig. 7). We will apply the displacement diagram method to only a small portion of the SAF system within the creeping segment of the fault near King City, California. For our analysis, we will calculate a displacement field for both distributed and discrete components of deformation along this segment of the SAF. Our calculations are based on the plate motion vector between the Pacific plate and the Sierra Nevada microplate (DeMets et al., 1990; Argus and Gordon, 2001), which provides the boundary conditions for the analysis. The present angle of convergence is approximately 6° clockwise from the SAF at the latitude of central California (Argus and Gordon, 2001), and the 39.0 mm/yr rate of convergence (Argus and Gordon, 2001) is resolvable into transcurrent (38.8 mm/yr) and shortening (4.1 mm/yr) components (Fig. 6). This plate motion vector has described the California margin since ~6–8 Ma (Harbert, 1991; Atwater and Stock, 1998), and we will limit our analysis to the last 6 M.y.

The SAF system contains multiple strands of parallel, strike-slip faults. In central California, the Rinconada and Hosgri–Nacimiento faults occur west of the main SAF (Fig. 7). Although total offset estimates exist for the Rinconada and San Gregorio–Hosgri faults (Graham and Dickinson, 1978; Sedlock and Hamilton, 1991), recent geodetic studies indicate that these faults are presently not accommodating more than 1 mm/yr of discrete transcurrent displacement (Argus and Gordon, 2001), while the SAF itself accommodates 34 mm/yr of transcurrent displacement.

Central California is a strike-slip partitioned transpressional system (e.g. Tikoff and Teyssier, 1994; Teyssier and Tikoff, 1998), in which the SAF accommodates a major portion, but not all, of the transcurrent displacement imposed by relative plate motion (e.g. Rymer et al., 1984; Prescott and Yu, 1986). The remaining motion occurs either as discrete displacement on sub-parallel strike-slip faults (e.g. San Gregorio–Hosgri, Rinconada faults) and/or as distributed displacement in the regions between the faults (e.g. en échelon folds in the regions between faults; Dibblee, 1976; Harding, 1976; Jamison, 1991; Tikoff and Peterson, 1998).

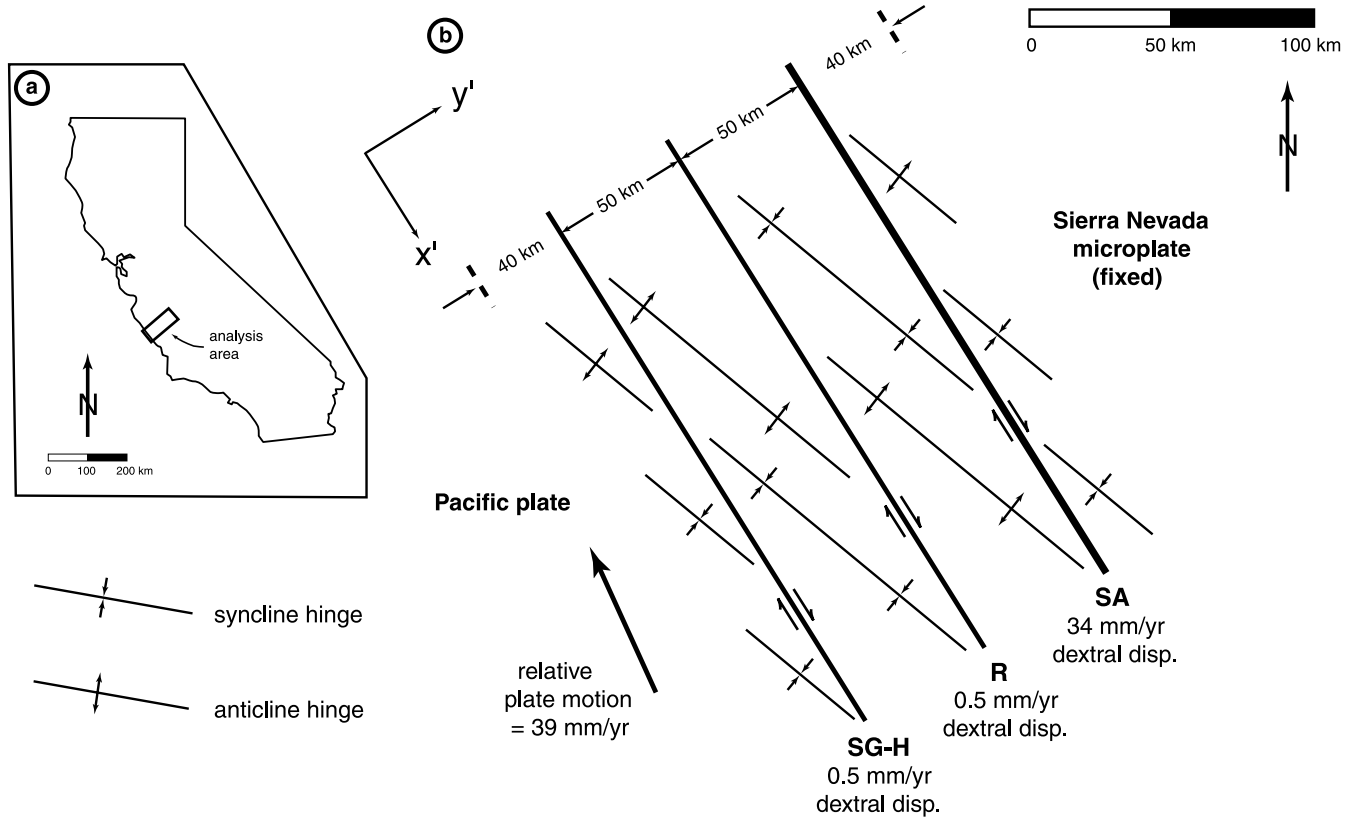

Fig. 7. A schematic diagram of the San Andreas Fault system in central California and the geodetic data for the relative motion between the Pacific plate and the Sierra Nevada microplate. (a) Map of California showing the location of the area analyzed. (b) A schematic map of the San Andreas Fault system in that area. We consider the entire region affected by transpression over the last 6 M.y. SG–H = San Gregorio–Hosgri fault, R = Rinconada fault, SA = San Andreas Fault.

6.4. Application of the technique

Prior to any analysis of the system, we establish a coordinate system to measure against and define the boundaries of the area we will analyze. In the interest of simplifying our calculations, we place the x' transect parallel to the trace of the SAF and the y' transect perpendicular to the SAF. We will consider a 180-km-thick (y'-parallel) transpressional region that has undergone deformation in the Neogene associated with the SAF (Fig. 7). The zone begins 40 km southwest of the San Gregorio–Hosgri fault and extends 40 km NE of the SAF. McCulloch (1989) outlines the limits of folding offshore SW of the San Gregorio–Hosgri fault and Namson and Davis (1988) outline the approximate limit of folding NE of the SAF.

We assume that western California is undergoing bulk transpressional deformation. The distributed component of this deformation narrows the thickness of the region as deformation progresses, which must be taken into consideration when calculating the displacement gradients for the system. Consequently, as above, we will first consider the distributed component of the deformation.

6.4.1. Distributed displacement

Because transpressional deformation occurs in the SAF system, two displacement diagrams are necessary to describe the deformation in the horizontal plane (i.e. $U_{x'}$ vs. y' and $U_{y'}$ vs. y'). A displacement diagram for $U_{x'}/x'$ is unnecessary because no fault-parallel, horizontal stretching occurs within the deforming zone. No displacement diagram for $U_{y'}$ vs. x' is necessary because motion perpendicular to the fault ($U_{y'}$) does not vary with position along the fault (x').

Estimation of the non-coaxiality of the distributed deformation within the borderlands requires assumptions about the rates of fault-parallel and -perpendicular displacement. As discussed above, geodetic estimates indicate that the SAF accommodates 34 mm/yr of transcurrent motion while the Rinconada and San Gregorio–Hosgri faults together accommodate 1 mm/yr. Therefore, the borderlands accommodate the remaining 3.8 mm/yr of the 38.8 mm/yr of transcurrent displacement. All of the 4.1 mm/yr of convergent displacement is accommodated by bulk shortening perpendicular to the SAF within the borderlands region.

As a first-order estimate for the last 6 M.y., we calculate forward displacements of $U_x = 22.8$ km (3.8 mm/yr over 6 M.y.—distributed fault-parallel displacement) and $U_y = -24.6$ km (-4.1 mm/yr over 6 M.y.—distributed fault-perpendicular displacement) within this 180-km-thick borderlands region. The fault-perpendicular

displacement can be used to determine the *initial* width of the region. We calculate that width of the deformed region was initially 180+24.6=204.6 km. Thus, the reciprocal distributed displacement gradients are:

$$\partial U_{x'}/\partial x' = 0, \tag{37a}$$

$$\partial U_{x'}/\partial y' = -22.8\ \text{km}/204.6\ \text{km} = -0.11, \tag{37b}$$

$$\partial U_{y'}/\partial x' = 0, \tag{37c}$$

$$\partial U_{y'}/\partial y' = 24.6\ \text{km}/204.6\ \text{km} = 0.12. \tag{37d}$$

In matrix form, these constitute the reciprocal distributed displacement gradient matrix:

$$\mathbf{H}_{\text{distributed}} = \begin{bmatrix} 0 & -0.11 \\ 0 & 0.12 \end{bmatrix}. \tag{38}$$

These displacement gradients are plotted on the appropriate reciprocal displacement diagrams in Fig. 8.

6.4.2. Discrete displacement

The amount of discrete offset across the SAF is estimated at 315 km, based on piercing point reconstructions (Crowell, 1962). Since we are interested only in deformation in the last 6 M.y., a total offset of only 204 km (34 mm/yr over 6 M.y.) is used. If the Rinconada and San Gregorio–Hosgri faults together accommodate 1 mm/yr of transcurrent motion, this suggests ~3 km of displacement on each fault over the last 6 M.y.

The above calculations are based on the assumption that current fault slip rates can be reasonably extrapolated back to 6 Ma. Using these geodetic measurements, we have calculated displacements on these faults for forward deformation over the last 6 M.y., such that:

$$U_x/x = 0, \tag{39a}$$

$$U_x/y = 204 + 3 + 3\ \text{km} = 210\ \text{km}, \tag{39b}$$

$$U_y/x = 0, \tag{39c}$$

$$U_y/y = 0. \tag{39d}$$

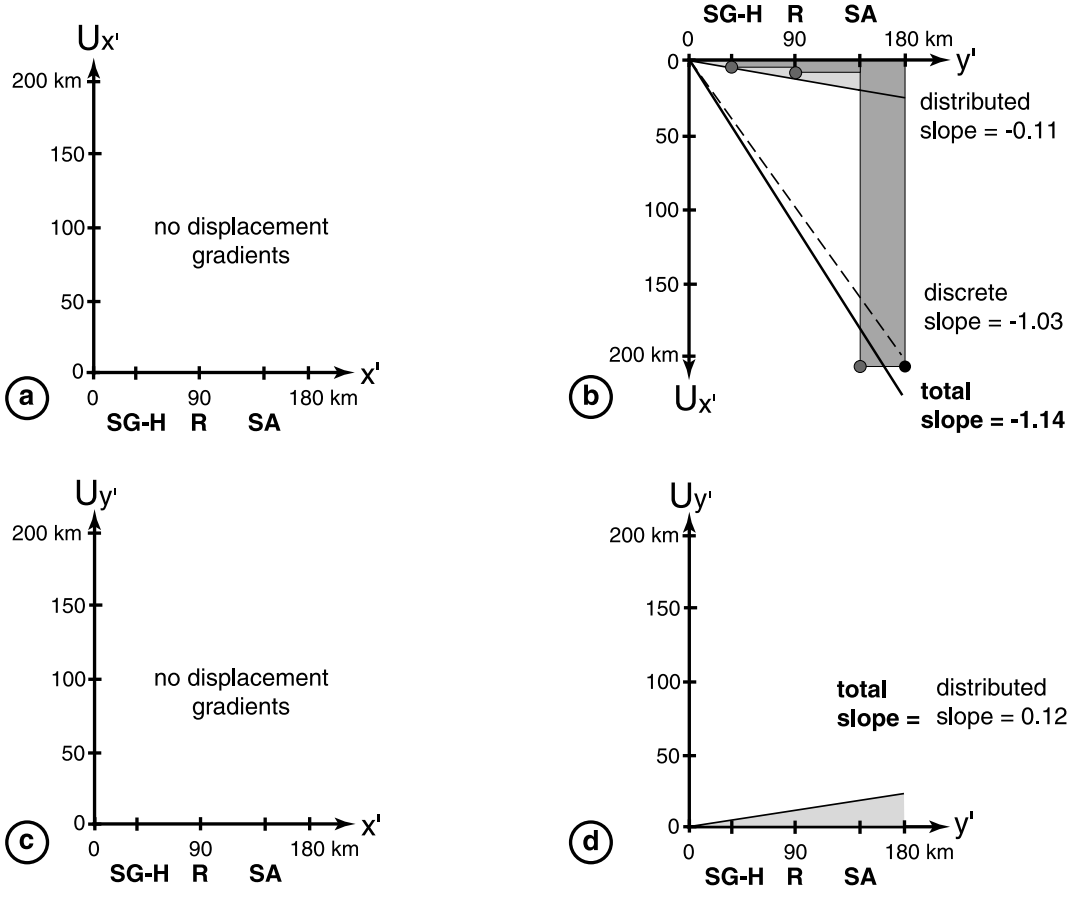

Fig. 8. Displacement diagrams for the creeping segment of the San Andreas Fault system, as shown in Fig. 7. Fault abbreviations are as in Fig. 7. (a) There is no displacement gradient in the x' direction as measured along the x' transect ($\partial U_{x'}/\partial x'$). (b) The large amount of discrete offset on the San Andreas Fault contributes to a large displacement gradient in the x' direction as measured along the y' transect ($\partial U_{x'}/\partial y'$). Dark gray boxes describe cumulative discrete displacement and the light gray area describes cumulative distributed displacement. (c) There is no displacement gradient in the y' direction as measured along the x' transect ($\partial U_{x'}/\partial x'$). (d) The displacement gradient in the y' direction as measured along the y' transect ($\partial U_{x'}/\partial y'$) is the result solely of distributed deformation in the transpressional borderlands.

As we are interested in reciprocal deformation, we must convert our calculated values into reciprocal displacements. This simply involves changing the sign of the displacement vectors. Normalizing the cumulative reciprocal displacement by the measured transect length results in the displacement gradients, which are plotted on displacement diagrams in Fig. 8. The reciprocal discrete displacement gradients are:

$$\partial U_{x'}/\partial x' = 0, \tag{40a}$$

$$\partial U_{x'}/\partial y' = (-204 + -3 + -3\ \text{km})/204.6\ \text{km} = -1.03, \tag{40b}$$

$$\partial U_{y'}/\partial x' = 0, \tag{40c}$$

$$\partial U_{y'}/\partial y' = 0. \tag{40d}$$

In matrix form, these constitute the reciprocal discrete displacement gradient matrix:

$$\mathbf{H}_{\text{discrete}} = \begin{bmatrix} 0 & -1.03 \\ 0 & 0 \end{bmatrix}. \tag{41}$$

6.4.3. Results of combined distributed and discrete deformation

Combining both the reciprocal discrete and distributed displacement gradients, we calculate the cumulative reciprocal displacement gradients, such that:

$$\partial U_{x'}/\partial x' = 0 + 0 = 0, \tag{42a}$$

$$\partial U_{x'}/\partial y' = -0.11 + -1.03 = -1.14, \tag{42b}$$

$$\partial U_{y'}/\partial x' = 0 + 0 = 0, \tag{42c}$$

$$\partial U_{y'}/\partial y' = 0.12 + 0 = 0.12. \tag{42d}$$

These calculations are plotted on the appropriate displacement diagrams in Fig. 8. The cumulative reciprocal displacement gradients, in matrix form, are:

$$\mathbf{H} = \mathbf{H}_{\text{discrete}} + \mathbf{H}_{\text{distributed}} = \begin{bmatrix} 0 & -1.03 \\ 0 & 0 \end{bmatrix} + \begin{bmatrix} 0 & -0.11 \\ 0 & 0.12 \end{bmatrix} = \begin{bmatrix} 0 & -1.14 \\ 0 & 0.12 \end{bmatrix}, \tag{43}$$

and the reciprocal deformation matrix is therefore:

$$\mathbf{E} = \mathbf{I} + \mathbf{H} = \begin{bmatrix} 1 & 0 \\ 0 & 1 \end{bmatrix} + \begin{bmatrix} 0 & -1.14 \\ 0 & 0.12 \end{bmatrix} = \begin{bmatrix} 1 & -1.14 \\ 0 & 1.12 \end{bmatrix}. \tag{44}$$

From **E** we calculate the deformation matrix:

$$\mathbf{D} = \mathbf{E}^{-1} = \begin{bmatrix} 1 & -1.14 \\ 0 & 1.12 \end{bmatrix}^{-1} = \begin{bmatrix} 1 & 1.02 \\ 0 & 0.89 \end{bmatrix}. \tag{45}$$

D describes the bulk deformation in central California, as observed in the horizontal plane, that has accumulated over the last 6 M.y. due to both the discrete and distributed components of the transpressional deformation.

Using this two-dimensional information, we can calculate the three-dimensional deformation matrix that describes this transpressional deformation. **D** describes a non-plane strain deformation. By calculating the determinant of **D**, we can quantify the amount of material that has moved out of the horizontal plane during the last 6 M.y. As $\det(\mathbf{D}) = 0.89$, we know that this horizontal plane has lost 11% of its area. Assuming that the system has not lost any volume, we conclude that this material has been displaced vertically. Therefore, we can calculate a three-dimensional deformation matrix by finding a **D** such that $\det(\mathbf{D}) = 1$. We find that this constraint is satisfied by

$$\mathbf{D} = \begin{bmatrix} 1 & 1.02 & 0 \\ 0 & 0.89 & 0 \\ 0 & 0 & 1.12 \end{bmatrix}, \tag{46}$$

which completely quantifies the bulk transpressional deformation in central California over the last 6 M.y.

On the scale of central California, the discrete component of deformation is accommodated completely on strike-slip faults. The distributed component accommodates all of the fault perpendicular shortening and a wrench component. On a smaller scale, the distributed component could be viewed as discrete offset, such as that occurring on regional faults. The folding observed in central California could, for instance, be caused by faulting at depth (e.g. Namson and Davis, 1988). Again, we note that the distinction between distributed and discrete deformation is scale-dependent. Regardless, the distributed component accommodates nearly 10% of the transcurrent motion ($U_{x'}/y'$ plot on Fig. 8). A shear strain of $\sim$0.11 constitutes $\sim$22.5 km ($=0.11\times180$ km) of distributed wrench motion in the last 6 M.y. across the entire region. We discuss implications of this distributed deformation in the Discussion section below.

7. Discussion

7.1. Potential applications

Bulk deformation of rocks is generally accommodated by a combination of distributed and discrete components over a wide range of scales. The methodology developed here is an initial attempt to characterize natural systems that behave in this manner. The ability to simultaneously characterize both

discrete and distributed deformation potentially allows us to address some key issues in structural geology, including strain compatibility, bulk offset analysis, and characterization of deformation in heterogeneous material. These kinematic approaches will ultimately lead us to better mechanical understanding of these systems.

A recurring problem in structural geology is the presence of shear zones whose kinematics deviate significantly from simple shear (e.g. Wallis, 1992; Bailey and Eyster, 2003). As pointed out in numerous articles, this leads to strain compatibility problems unless the walls of the shear zones are also deformed. Hudleston (1999) suggested that the problem of strain compatibility caused by non-simple shear zones is significantly alleviated by considering anastomosing shear zones and deforming lithons between the shear zones. The methodology outlined in this paper provides one means for rigorously testing this model.

The displacement diagram method also makes it possible to quantify deformation of heterogeneous material. The heterogeneous nature of geological deformation is an inevitable result of lithological heterogeneity. As suggested by Goodwin and Tikoff (2002), lithological heterogeneity and competence contrast within a polyphase material lead to strain incompatibilities that result in discrete deformation at some scale. Using the displacement diagram method, strain heterogeneity can be adequately characterized because of the flexibility of displacements to describe these systems. Displacement diagrams are useful tools for analyzing heterogeneous deformation because displacement field inhomogeneity is graphically (and quantitatively) apparent on displacement diagrams as changes in displacement gradients.

The method also allows clear mechanical insight into a deformed system by evaluating the relative contribution of discrete and distributed components. For over a decade, there has been a debate about the strength of the San Andreas Fault (Mount and Suppe, 1987; Zoback et al., 1987; Scholz, 2000). Our first-order kinematic analysis suggests that a significant percentage of transcurrent motion is distributed over central California rather than occurring on a discrete fault. In our opinion, this is incompatible with a 'weak' fault that should presumably accommodate all the transcurrent motion. This approach allows us to quantify observations, which in turn will allow increasingly accurate mechanical models based on direct observation.

7.2. Problems and assumptions

General application of the displacement diagram method is complicated by the fact that a large amount of information is required to properly analyze a deformed zone. Analysis of the discrete portion of deformation requires knowledge of the original fault geometry, sufficiently abundant offset markers and an independent estimate of rotation (shear-induced vorticity). Analysis of the distributed deformation is more difficult as many shear zones lack adequate vorticity and/or finite strain indicators. Consequently, at present, this method will be most useful for well-constrained deformation zones.

Some possible complications are inherent in the interpretation of results from the displacement diagram method. The results of the method depend strongly on the choice of transect orientations and lengths. Consequently, the selection of appropriate, representative transects is essential. The problem of the changing thickness of the deforming zone requires that one transect be inscribed parallel to the deformed system's bulk shear plane. The changing thickness of the zone can then be thoroughly quantified, provided the system has a constant volume, by analyzing the pure shear component of deformation.

Additionally, transect length must be considered carefully as it can dramatically affect displacement gradient results. The simplest approach to determining appropriate transect lengths is to measure displacements along the entire width of a deformed zone, as we did for the San Andreas Fault system example. In many cases, however, the full extent of a deformed zone may be unknown. One approach is to select clear boundaries for the analysis zone. For example, consider a large deformed region dissected by faults. Choosing some of these faults as arbitrary boundaries and analyzing all deformation inside (and exclusive of) these faults will provide an estimate of the deformation of that relatively small region. Ideally, deformation in this region might reasonably be considered representative of deformation in the entire system and the results could be extrapolated to the entire system.

The displacement diagram method assumes the simultaneous activation of the discrete and distributed components of deformation. If discrete deformation, such as faulting, postdates distributed deformation (or vice versa), a sequential approach to retrodeformation is necessary. One complication arising from simultaneous activity of discrete and distributed components is that displacement on faults may be due to both straightforward fault slip and to offset resulting from differential finite strain in blocks adjacent to the fault (as in Fig. 6c).

The method also assumes that deformation of material is steady-state. That is, the deformation could have stopped and started in time, but when deformation was ongoing it was accumulating with the same deformation path (ratio of stretching rate to shear induced vorticity rate). The difficulties with the assumption of steady-state deformation are somewhat alleviated by considering bulk deformation paths (directly analogous to the bulk vorticity of Passchier (1988)).

8. Conclusions

The strain in a deformed system, as accommodated by both discrete and distributed components of deformation, can be quantified using the displacement diagram method (Wojtal, 1989). These components plot as two distinct displacement gradients on a displacement diagram. The sum of the two component displacement gradients yields a bulk

displacement gradient. In the absence of simplifying assumptions, four displacement diagrams are necessary to describe a two-dimensional deformation and nine are necessary to describe a three-dimensional deformation. From a matrix composed of displacement gradients calculated from these diagrams, a deformation matrix describing the bulk deformation can be determined.

The method is very flexible insofar as one can analyze deformations using finite information (finite strain, offsets), displacement rates (geodetic measurements), and/or combinations of the two. The method works best when there is a significant amount of information about the boundary conditions of deformation. Three major limitations to the method are the ability to evaluate (1) the rotation (shear-induced vorticity) for the distributed deformation, (2) the original fault geometry and spacing, and (3) the relative importance of offset on discrete surfaces due to differential finite strain in the adjacent blocks vs. straightforward fault slip.

The displacement diagram method allows a robust characterization of complex natural systems. The simplicity of this method, in terms of both data collection and analysis, and its scale independence makes it applicable to a wide range of deformations.

Acknowledgements

We thank Steve Wojtal and Laurel Goodwin for encouraging, helpful discussions. Eric Ferré provided the photomicrograph of the S–C fabric in the Sandkraal sandstone. The manuscript was much improved following reviews by and discussions with Scott Giorgis, Sarah Tindall, Sarah Titus and Cheryl Waters. Marcia Bjornerud and Dan Schultz-Ela provided thorough, critical reviews and we thank them.

Appendix A. Calculation of finite strain from displacement gradients

This appendix outlines the procedure for calculation of some common measures finite strain from displacement gradients. This procedure is the same regardless of the number of dimensions being analyzed. For simplicity, we present the procedures in two dimensions.

The reciprocal deformation matrix **E** describes the transformation of the system from the deformed to the undeformed state. **E** is calculated by adding the identity matrix **I** to the matrix of reciprocal displacement gradients **H**. These operations are as follows:

$$\mathbf{E} = \mathbf{I} + \mathbf{H} \tag{A1a}$$

$$\mathbf{E} = \begin{bmatrix} 1 & 0 \\ 0 & 1 \end{bmatrix} + \begin{bmatrix} \partial U_{x'}/\partial x' & \partial U_{x'}/\partial y' \\ \partial U_{y'}/\partial x' & \partial U_{y'}/\partial y' \end{bmatrix} \tag{A1b}$$

$$\mathbf{E} = \begin{bmatrix} 1 + \partial U_{x'}/\partial x' & \partial U_{x'}/\partial y' \\ \partial U_{y'}/\partial x' & 1 + \partial U_{y'}/\partial y' \end{bmatrix} \tag{A1c}$$

The matrix inverse of **E** is the deformation matrix **D**, which describes the transformation of the system from the undeformed to the deformed state:

$$\mathbf{D} = \mathbf{E}^{-1} = \begin{bmatrix} 1 + \partial U_x/\partial x & \partial U_x/\partial y \\ \partial U_y/\partial x & 1 + \partial U_y/\partial y \end{bmatrix} \tag{A2}$$

Many standard measures of finite strain can be calculated from **D** using linear algebra procedures. For example, the principal strain values of the strain ellipse (S_1 and S_2 are the square roots of the eigenvalues of $\mathbf{DD}^{\mathrm{T}}$, where $\mathbf{D}^{\mathrm{T}}$ is the transpose of **D**:

$$\mathbf{DD}^{\mathrm{T}} = \begin{bmatrix} 1 + \partial U_x/\partial x & \partial U_x/\partial y \\ \partial U_y/\partial x & 1 + \partial U_y/\partial y \end{bmatrix} \begin{bmatrix} 1 + \partial U_x/\partial x & \partial U_y/\partial x \\ \partial U_x/\partial y & 1 + \partial U_y/\partial y \end{bmatrix} \tag{A3}$$

$$= \begin{bmatrix} (1 + \partial U_x/\partial x)^2 + (\partial U_x/\partial y)^2 & (1 + \partial U_x/\partial x)(\partial U_y/\partial x) + (\partial U_x/\partial y)(1 + \partial U_y/\partial y) \\ (\partial U_y/\partial x)(1 + \partial U_x/\partial x) + (1 + \partial U_y/\partial y)(\partial U_x/\partial y) & (1 + \partial U_y/\partial y)^2 + (\partial U_y/\partial x)^2 \end{bmatrix} \tag{A4}$$

$$\times S_1 \text{ and } S_2 = \sqrt{\text{eigenvalues}(\mathbf{DD}^{\mathrm{T}})}$$

S_1 and S_2 are the magnitudes of the principal strain axes of the deformation imposed by **D**. The orientations of these axes are described by the eigenvectors that correspond to each eigenvalue.

All common measures of finite strain can be calculated from **D**. Ramsay and Huber (1983, their Appendix B) describe the straightforward procedures for calculation of many of these measures.

Appendix B. Forward vs. reciprocal approaches

Considered from different perspectives, Fig. 2a and d represents the same deformation. Fig. 2a represents the deformation in a forward modeling sense, moving from the

undeformed (dashed line) to the deformed (solid line) state. This approach is occasionally called the *Lagrangian* viewpoint (Ramsay and Huber, 1983, p. 283). In contrast, Fig. 2d represents the reciprocal deformation. The approach treats the deformed state as the reference configuration (dashed line) that is altered to the undeformed state (solid line). This is the *Eulerian* viewpoint (Ramsay and Huber, 1983, p. 283), which is required for the direct analysis of naturally deformed rocks.

We refer to these two approaches, respectively, as the *forward* and *reciprocal* (or inverse) models of deformation, illustrated in Fig. 3. The forward or Lagrangian approach assumes knowledge of the initial material position and deformation matrix **D** (Fig. 3a). If one determines a partitioning coefficient between the distributed and discrete components of deformation (Fig. 3b), one can determine the displacement gradients (Fig. 3c), components of discrete and distributed deformation (Fig. 3d), and the resultant deformation (Fig. 3e). This approach is essentially that of Tikoff and Teyssier (1994), who modeled the partitioning of bulk transpressional deformation into discrete and distributed components. The difficulties of this approach are twofold:

1. *Non-uniqueness*—Forward modeling creates predictions that are comparable with geological observations, but does not analyze the geological structures themselves. Consequently, there is a problem with non-uniqueness. Geological structures may be consistent with the kinematic models, but may have actually formed by completely different kinematics. This situation is potentially avoided by using multiple lines of evidence.
2. *Prescribed boundary conditions*—The forward method requires ad hoc methods of determining the exact boundary conditions, such as the relative percentage of distributed vs. discrete deformation (e.g. Tikoff and Teyssier, 1994). However, geological observations can help guide the prescription of these boundary conditions.

We note that these limitations occur for any type of forward model, including both kinematic and dynamic varieties.

In contrast, the reciprocal approach uses geological observations as the basis for the deformation analysis (Fig. 3e). This method uses the observed geometry (Fig. 3f) to determine the components of distributed and discrete deformation (Fig. 3g). Displacement gradients (Fig. 3h) are calculated from finite strain, or directly from measured displacements, which allows one to calculate the reciprocal strain (Fig. 3h).

This approach is potentially superior to the forward model, because it is based on actual deformation rather than conceptual models. Reciprocal models of deformation are inherently kinematic, as these are the only direct observations that are obtained. The major impediment to this approach is obtaining sufficiently accurate data to allow quantitative analysis.

References

Argus, D.F., Gordon, R.G., 2001. Present tectonic motion across the Coast Ranges and San Andreas fault system in central California. Geological Society of America Bulletin 113, 1580–1592.

Atwater, T., Stock, J., 1998. Pacific–North America plate tectonics of the Neogene southwestern United States: an update. In: Ernst, W.G., Nelson, C.A. (Eds.), Integrated Earth and Environmental Evolution of the Southwestern United States. Bellwether Publishing, pp. 393–420.

Bailey, C.M., Eyster, E.L., 2003. General shear deformation in the Pinaleño Mountains metamorphic core complex, Arizona. Journal of Structural Geology 25, 1883–1892.

Bobyarchick, A.R., 1986. The eigenvalues of steady flow in Mohr space. Tectonophysics 122, 35–51.

Cobbold, P., 1977. Description and origin of banded deformation structures, I: regional strain, local perturbations, and deformation in bands. Canadian Journal of Earth Science 14, 1721–1731.

Crowell, J.C., 1962. Displacement along the San Andreas fault, California. Geological Society of America Special Paper 71, 61pp.

Daczko, N.R., Klepeis, K.A., Clarke, G.L., 2001. Evidence of Early Cretaceous collisional-style orogenesis in northern Fiordland, New Zealand and its effects on the evolution of the lower crust. Journal of Structural Geology 23, 693–713.

DeMets, C., Gordon, R.G., Argus, D.F., Stein, S., 1990. Current plate motions. Geophysical Journal International 101, 425–478.

Dibblee, T.W., 1976. The Rinconada and related faults in the southern Coast Ranges, California, and their tectonic significance. U.S. Geological Survey Professional Paper 981, 55pp.

Elliott, D., 1972. Deformation paths in structural geology. Geological Society of America Bulletin 83, 2621–2635.

Erskine, B.G., Heidelbach, F., Wenk, W.-R., 1993. Lattice preferred orientations and microstructures of deformed Cordilleran marbles: correlation of shear indicators and determination of strain path. Journal of Structural Geology 15, 1189–1205.

Fossen, H., Tikoff, B., 1993. The deformation matrix for simultaneous pure shear, simple shear, and volume change, and its application to transpression/transtension tectonics. Journal of Structural Geology 15, 413–425.

Ghosh, S.K., 1987. Measure of non-coaxiality. Journal of Structural Geology 9, 111–113.

Goodwin, L.B., Tikoff, B., 2002. Competency contrast, kinematics, and the development of foliation and lineation in the crust. Journal of Structural Geology 24, 1065–1085.

Graham, S.A., Dickinson, W.R., 1978. Evidence for 115 kilometers of right slip on the San Gregorio–Hosgri fault trend. Science 199, 179–181.

Harbert, W., 1991. Late Neogene relative motions of the Pacific and North American plates. Tectonics 10, 1–16.

Harding, T.P., 1976. Tectonic significance and hydrocarbon trapping consequences of sequential folding synchronous with San Andreas faulting, San Joaquin Valley, California. A.A.P.G. Bulletin. v60 n3, pp. 356–378.

Hudleston, P.J., 1999. Strain compatibility in shear zones: is there a problem? Journal of Structural Geology 21, 923–932.

Jamison, W.R., 1991. Kinematics of compressional fold development in convergent wrench terranes. Tectonophysics 190, 209–232.

Law, R.D., Knipe, R.J., Dayan, H., 1984. Strain path partitioning within thrust sheets: microstructural and petrofabric evidence from the Moine thrust at Loch Eriboll, northwest Scotland. Journal of Structural Geology 6, 477–497.

Lister, G.S., Williams, P.F., 1983. The partitioning of deformation in flowing rock masses. Tectonophysics 92, 1–33.

Little, T., 1996. Faulting-related displacement gradients and strain adjacent to the Awatere strike-slip fault in New Zealand. Journal of Structural Geology 18, 321–342.

Luyendyk, B.P., 1991. A model for Neogene crustal rotations, transtension, and transpression in southern California. Geological Society of America Bulletin 103, 1528–1536.

Marrett, R., Allmendinger, R., 1990. Kinematic analysis of fault-slip data. Journal of Structural Geology 12, 973–986.

McCulloch, D.S., 1989. Evolution of the offshore central California margin. In: Winterer, E.L., Hussong, D.M., Decker, R.W. (Eds.), The Geology of North America, v. N. The Eastern Pacific Ocean and Hawaii. The Geological Society of America, Boulder CO, pp. 439–470.

Means, W.D., 1976. Stress and Strain: Basic Concepts of Continuum Mechanics for Geologists. Springer-Verlag, New York. 339pp.

Mount, V.S., Suppe, J., 1987. The state of stress near the San Andreas fault: implications for wrench tectonics. Geology 15, 1143–1146.

Namson, J.S., Davis, T.L., 1988. Seismically active fold and thrust belt in the San Joaquin Valley, Central California. Geological Society of America Bulletin. v100, n2, pp. 257–273.

Passchier, C.W., 1988. The use of Mohr circles to describe non-coaxial progressive deformation. Tectonophysics 149, 323–338.

Passchier, C.W., Urai, J.L., 1988. Vorticity and strain analysis using Mohr diagrams. Journal of Structural Geology 10, 755–763.

Prescott, W.H., Yu, S.-B., 1986. Geodetic measurement of horizontal deformation in the northern San Francisco Bay region, California. Journal of Geophysical Research 86, 7475–7484.

Ramsay, J., Huber, M., 1983. The Techniques of Modern Structural Geology. Volume 1: Strain Analysis. Academic Press, San Diego. 307pp.

Rouby, D., Cobbold, P., Szatmari, P., Demerican, S., Coehlo, D., Rici, J., 1993. Least-squares palinspastic restoration of regions of normal faulting—application to the Campos basin (Brazil). Tectonophysics 221, 439–452.

Rymer, M.J., Lisowski, M., Burford, R.O., 1984. Structural explanation for low creep rates on the San Andreas fault near Monarch Peak, Central California. Bulletin of the Seismological Society of America 74, 925–931.

Scholz, C.H., 2000. Evidence for a strong San Andreas Fault. Geology 28, 163–166.

Sedlock, R.L., Hamilton, D.H., 1991. Late Cenozoic tectonic evolution of southwestern California. Journal of Geophysical Research 96, 2325–2351.

Simpson, C., De Paor, D.G., 1993. Strain and kinematic analysis in general shear zones. Journal of Structural Geology 15, 1–20.

Srivastava, H.B., Hudleston, P., Earley, D., 1995. Strain and volume loss in a ductile shear zone. Journal of Structural Geology 17, 1217–1231.

Teyssier, C., Tikoff, B., 1998. Strike-slip partitioned transpression of the San Andreas fault system: a lithospheric scale approach, in: Holdsworth, R.E., Strachan, R.A., Dewey, J.F. (Eds.), Continental Transpressional and Transtensional Tectonics Geological Society of London Special Publication, 135, pp. 143–158.

Thatcher, W., 1995. Microplate vs. continuum descriptions of active tectonic deformation. Journal of Geophysical Research 100, 3885–3894.

Tikoff, B., Fossen, H., 1995. Limitations of three-dimensional kinematic vorticity analyses. Journal of Structural Geology 17, 1771–1784.

Tikoff, B., Peterson, K., 1998. Physical models of transpressional folding. Journal of Structural Geology 20, 661–672.

Tikoff, B., Teyssier, C., 1994. Strain modeling of displacement–field partitioning in transpression orogens. Journal of Structural Geology 16, 1575–1588.

Truesdell, C., 1953. Two measures of vorticity. Journal of Rational Mechanical Analysis 2, 173–217.

Vissers, R.L.M., 1989. Asymmetric quartz c-axis fabrics and flow vorticity: a study using rotated garnets. Journal of Structural Geology 11, 231–244.

Wallis, S.R., 1992. Vorticity analysis in metachert from the Sanbagawa Belt, SW Japan. Journal of Structural Geology 14, 271–280.

Wojtal, S., 1989. Measuring displacement gradients and strains in faulted rocks. Journal of Structural Geology 11, 669–678.

Zoback, M.D., Zoback, M.L., Mount, V.S., Suppe, J, Eaton, J.P., Healy, J.H., Oppenheimer, D.H., Reasenberg, P.A., Jones, L.M., Raleigh, C.B., Wong, I.G., Sotti, O., Wentworth, C.M., 1987. New evidence of the state of stress of the San Andreas fault system. Science. v238, n4830, pp. 1105–1111.